

Variability of erodibility in bedrock-floored channels produced by differential weathering

A thesis submitted in partial fulfillment of the requirements
for the degree of Bachelor of Science in Geology from
the College of William and Mary

by

Matthew S. Sparacino

Accepted for _____
(Honors, High Honors)

Dr. Gregory S. Hancock, Director

Dr. James M. Kaste

Dr. Mark K. Hinders

Williamsburg, Virginia
April 26, 2012

Table of Contents

Table of Contents	2
List of Figures	3
List of Tables	3
Abstract	4
Introduction.....	5
Methods.....	12
Results.....	24
Discussion	39
Conclusion	50
Future Work	51
Acknowledgements.....	52
References.....	53
Appendix	
A: Transect Survey, Schmidt Hammer, and Channel Geometry Data.	58

List of Figures

1. Channel geometry concept diagram.....	9
2. Shaded relief maps with field site locations.	15
3. Sample site photos with transect overlays.	17
4. Schmidt hammer values vs. elevation above thalweg	25
5. Width vs. depth for all channels	29
6. Weight percent elemental oxides, site A.....	31
7. Chemical weathering indices and percent porosity, site A	32
8. Weight percent elemental oxides, site B	34
9. Chemical weathering indices and percent porosity, site B	35
10. Weight percent elemtal oxides, site F.....	377
11. Chemical weathering indices and percent porosity, site F.....	38
12. 1.0 m pore space fase color image, site F	40
13. 0 m rock core, site A	43
14. 1.1 m silicadistribution map, site B	45
15. Photo of 0.1m transect at Virginia limestone, site B	46

List of Tables

1. Sample Site Characteristics	18
2. Schmidt hammer data by channel site	26

Abstract

The erosion of bedrock-floored channels is a critical process governing the rate of landscape evolution in many settings. Recent numerical modeling of rock-floored channel cross-sections suggests that equilibrium channel geometry and slope are sensitive to variations in rock erodibility, especially along the channel perimeter. However, few field studies have focused on systematic measurement of rock erodibility across bedrock-floored channels. We hypothesize that variations in weathering intensity and duration across some channels results in variable erodibility. To determine if erodibility varies in some channels, we used a Type N SilverSchmidt hammer to measure *in situ* compressive strength in channels floored by sandstone (3 sites, Utah), granite (1 site, Virginia) and limestone (2 sites, Virginia). Rock strength, which decreases with increased weathering, is assumed to be an adequate proxy for erodibility (Sklar et al., 2001). In four of six channels, average compressive strength decreased 24 – 52% between the waterline and the highest exposed bedrock (1.6 – 3.2 m above the thalweg). In one limestone channel, average compressive strength increased 70% between the waterline and 2.6 m above the thalweg. In a rapidly eroding sandstone channel, erodibility remained constant at all elevations. We used an electron microprobe to conduct chemical weathering and porosity analyses on three of five channels. Observed variation in bedrock erodibility is predominantly caused by weathering, but the extent and dominant form are highly variable, depending on climate conditions and rock type.

Introduction

The erosion of bedrock-floored river channels is an essential process controlling the evolution of landscapes, especially in mountainous and tectonically uplifting areas, where slopes are generally too steep to allow for significant sediment deposition (Whipple, 2004). In these environments, bedrock channels provide the primary, non-glacial mechanism for bedrock erosion (Hancock et al., 1998). Bedrock river channels determine the denudation rates and patterns of surrounding hillslopes by: 1) setting the boundary conditions to which hillslopes can erode (Burbank et al., 1996), 2) transferring changes caused by climatic and tectonic forcing through landscapes (Whipple, 2001; Bishop et al., 2005; Berlin and Anderson, 2007; Finnegan et al., 2007), and 3) ultimately controlling the rates at which landscapes respond to perturbations (Whipple and Tucker, 1999; Whipple, 2001). Despite the importance of bedrock channels in regulating landscape change, our understanding of the rates and spatial distribution of erosion within bedrock channels remains incomplete. In order to develop better bedrock channel evolution models, more field data is required to quantify the extent to which various factors influence channel erosion.

The individual processes that contribute to bedrock channel incision have been well studied (e.g., Foley, 1980; Seidl and Dietrich, 1992; Hancock et al., 1998). Erosion is predominantly achieved through a combination of suspended and bed load abrasion, block plucking, and, possibly, cavitation. The efficacy of these processes depends on complex relationships between localized channel flow conditions and rock properties; including channel geometry, gradient, and the frequency distribution of floods (Wobus et al., 2006), sediment load and cover (Sklar and Dietrich, 2001; Turowski et al., 2009), and

the cross channel distribution of substrate erodibility, which may be affected by lithological differences and rock degradation through physical and chemical weathering (Montgomery, 2004; Stock et al., 2005). In modeling bedrock channel evolution, these factors are condensed into the simplified, but widely used shear stress erosion law:

$$E = KA^m S^n \quad (1)$$

where E is the total erosion due to all processes, K is a dimensionless bedrock-specific erodibility factor, A is upstream drainage area (proxy for discharge), S is channel gradient, and m and n are positive constants that depend on erosion process, basin hydrology, and channel hydraulic geometry (Howard et al., 1994). Erodibility has a significant effect on the predominance of various erosive mechanisms, but this K variable incorporates all factors that control erodibility. A limitation of this equation exists in its inability to quantify the effects of spatially variable erodibility on erosion in a channel.

The shear stress erosion law (Eq. 1) is based on the assumption that bedrock erosion scales with the power-law function of mean bed shear stress (Howard and Kerby, 1983). Recent modeling by Turowski et al. (2008a) suggests that a non-uniform distribution of shear stress exists across bedrock channels, where shear stress is concentrated in the channel center during low flows and the margins during high flows. Many landscape evolution models disregard the possibility of a transient cross-sectional geometry, and address fluvial down cutting as the only channel response to ambient tectonic and hydrologic conditions (Turowski et al., 2008a). Some models have shown that channels adjust their width as well as, and sometimes instead of, channel slope, in response to changing sediment supply, discharge, and rock uplift (Turowski et al., 2008b; Duvall et al., 2004; Wobus et al., 2006). Other models suggest that shear stress is

constantly redistributed as geometry changes while the channel adjusts toward an equilibrium state, at which point channel incision lowers a stable cross section through time (Wobus et al., 2006; Stark, 2006). While this self-formed channel evolution model is based on the shear stress equation (Eq. 1) that includes a bedrock erodibility factor, it assumes that the bedrock throughout the channel cross section has the same erodibility.

The idea of cross-channel equal erodibility is a significant limitation as cross-channel variation in erodibility may be related to bedrock weathering and lithological variation. Whipple (2004) suggests that weathering processes weaken and prepare the channel bed for erosion. Turowski et al. (2009) agree, but stress the need for a better understanding of the role of substrate properties and weathering on channel development. Weathering lowers rock cohesion, which lowers rock frictional strength, which leads to significantly higher erosion rates in weathered rock samples compared to unweathered samples of the same rock type (Selby, 1980; Sklar and Dietrich, 2001). Lab studies have found that weathered sandstone can erode several orders of magnitude faster than unweathered sandstone, while weathered granite can erode up to an order of magnitude faster than unweathered granite (Sklar and Dietrich, 2001). Weathering processes depend upon a variety of environmental and substrate conditions, and those that are enhanced by periodic water exposure may be more effective on channel margins as opposed to the channel center, including: biological weathering caused by plant colonization of fresh bedrock (Phillips et al., 2008); frost shattering (e.g. Anderson, 1998); oxidation of iron bearing minerals; and mineral hydration during wetting/drying cycles (Stock et al., 2005). Fracture density and porosity increase the efficacy of many weathering processes, and rock type dictates which weathering processes are most dominant (Whipple, 2004). In

areas where bedrock type and climate yield significant weathering, this weathering can serve to increase the erodibility of bedrock exposed on the margins, above the common flow height, causing it to erode during larger flows (Montgomery, 2004; Stock et al., 2005). Although rock in the channel center may be weathering at the same rate or faster than bedrock on the margins, bedrock in the center is constantly eroded by frequent, low flows. The resulting spatial variation in rock erodibility may allow a lower shear stress along the channel margins to erode bedrock at the same rate or faster than the channel center; a reduction of the shear stress required along the channel margins to maintain channel equilibrium may alter the channel's equilibrium geometry (Hancock et al., 2011).

The geometry and gradient of bedrock-floored channels are critical controls on the rate of bedrock erosion because they influence: 1) the rate of energy loss as water moves through a cross-section; 2) the distribution of velocity and shear stress within a channel; and 3) ultimately, the distribution of erosive power across the channel. Recent modeling suggests that weathering may change the distribution of erodibility, with significant effects on bedrock channel geometry and slope (Hancock et al., 2011). Hancock et al. (2011) found that where uniform erodibility exists in channels subjected to low uplift rates (where weathering outpaces erosion) and high uplift rates (where erosion everywhere outpaces weathering), there is little to no change in width-to-depth ratio relative to channels that do not weather (Figure 1). At intermediate uplift rates, weathering increases rock erodibility on channel margins relative to the channel center, resulting in width-to-depth ratios up to ~ 50% greater than in channels with uniform erodibility (Hancock et al., 2011).

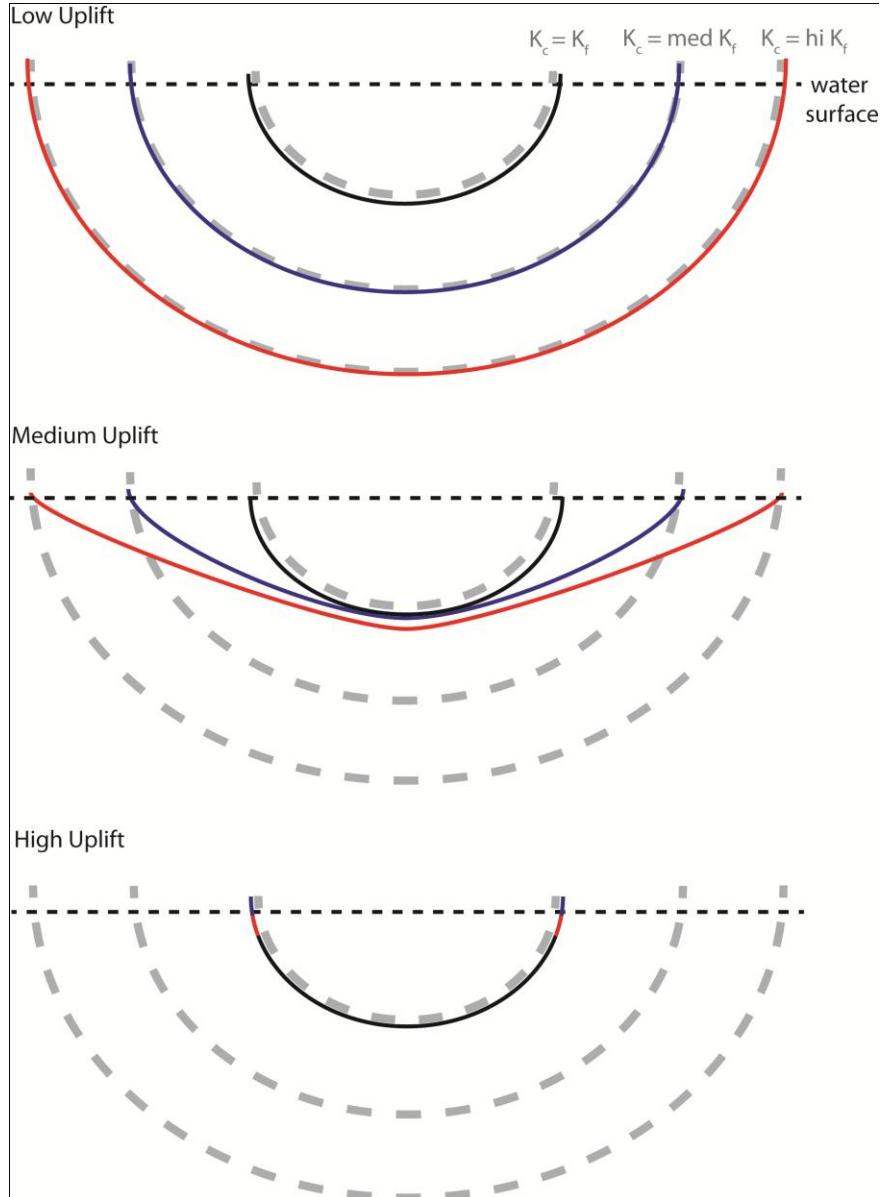


Figure 1: Dashed gray lines represent channel cross sections produced by channels with fixed erodibility, where increasing channel size is related to increasing erodibility. Solid lines represent channel cross sections with initial erodibility $K_c = K_f$, but where weathering has increased rock erodibility to *med* K_f or *hi* K_f . At a low uplift rate (where uplift refers to any lowering of base level), all bedrock in the channel cross section has time to fully weather, resulting in channels with similar geometry at all levels of erodibility. At a medium uplift rate, bedrock on the margins has time to fully weather, while bedrock in the thalweg is eroded faster than it can weather. As extent of weathering increases, channels widen faster than they incise vertically. At a high uplift rate, all bedrock in the channel cross section is eroded before it has time to weather. This produces channels with similar geometry at all levels of rock erodibility. (After Hancock et al., 2011)

Aside from recent work done for two undergraduate theses, field studies aimed at analyzing the variation in erodibility across bedrock channels or the connection between weathering and rock erodibility have not been undertaken. Murphy's thesis found that rock strength decreased and became more variable with increasing height above the channel thalweg, but he found limited evidence linking weathering to decreasing rock strength. Lamp improved Murphy's methods with a wider and more systematic collection of Schmidt hammer data as well as increased sampling for extent of chemical weathering. She found similar variations in erodibility across many of the sampled channels and made initial observations that this variation may be a result of differential weathering. Lamp suggests sampling channels in a wider range of hydro-climatic conditions and additional development of the methods used to measure the extent of chemical weathering. Hancock et al. (2011) propose field tests to identify if erodibility is spatially variable across natural channels (using abrasion mills) and to identify the impact of weathering (quantifying rock mass strength). In order to identify if weathering is responsible for producing variable erodibility, the extent of weathering needs to be evaluated wherever erodibility is measured. The relationship between channel geometry and erodibility of the channel perimeter in the field should be compared to the model results. Since weathering is the only mechanism to promote increasing width-to-depth ratio in the Hancock et al. (2011) model, measurements of channel geometry and erodibility should target areas where lithology and external controls on weathering (e.g. climate) remain constant (Hancock et al., 2011).

We present the results of a field and lab based study, focused on collecting direct measurements of erodibility and weathering extent in natural, bedrock-floored channels.

We address the following questions:

- 1) does erodibility vary across rock-floored channels?
- 2) is weathering responsible for variations in erodibility?

Methods

Estimating Rock Erodibility

The Schmidt hammer, initially designed for concrete testing, is now being used to determine the hardness of rock surfaces in the field (Day, 1980; Selby, 1980). We use a Type N SilverSchmidt hammer as a measure of *in situ* compressive strength across bedrock-floored channel cross sections. The Schmidt hammer provides a relative measure (Q-value) of the compressive strength of rock by measuring the rebound distance of a metal plunger after it impacts a rock surface (Goudie, 2006). The Schmidt hammer records Q-values between 13.5 (low compressive strength) and 80 (high compressive strength). Since erodibility has been shown to increase with decreasing rock tensile strength (Sklar and Dietrich, 2001) as well as with decreasing compressive strength (Suzuki and Takahashi, 1981), we use the Schmidt hammer measure of compressive strength as a proxy for erodibility. The Schmidt hammer is commonly used to measure the degree of rock surface weathering (Matthews and Shakesby, 1984; Ballantyne et al., 1989). These studies measured large scale differences on a wide array of boulders in multiple periglacial environments and found a strong negative correlation between rebound values and the degree of rock weathering. Weathering decreases rock strength, which allows the rock to absorb more of the impact, resulting in lower rebound values (Day and Goudie, 1977; Sumner and Nel, 2002). Gupta et al. (2011) found that the variability of Schmidt hammer values also increases with increasing weathering, which they attribute to significant surface roughness caused by differential weathering of mineral grains.

While the Schmidt hammer is generally recognized as a convenient technique for preliminary weathering assessments, all differences in rebound values cannot simply be assigned to differences in weathering (McCarroll, 1991). There are a number of lithological and rock surface characteristics that affect rebound values and potentially limit the tool's accuracy, so any Schmidt hammer study focused on weathering must account for these effects (Day, 1980; Williams and Robinson, 1983). The differential weathering of mineral grains in heterogeneous rocks often increases surface roughness on the sub-centimeter scale, which results in lower Schmidt hammer values than smooth surfaces, and in a wider range of rebound values (Williams and Robinson, 1983; McCarroll, 1989; Gupta et al., 2011). Increased surface roughness decreases the rock area at the contact point with the Schmidt hammer and lowers the local rock mass, which allows energy to dissipate through edges rather than return to the hammer. Similarly, highly fractured, bedded, and fissile rocks return lower Schmidt hammer values than massive rocks (Goudie, 2006). Moisture content is related to rock properties such as porosity and permeability, so its effect on Schmidt hammer rebound values varies significantly between rock types. Sumner and Nel (2002) sampled five rock types and found that sandstones had the greatest moisture uptake, resulting in a maximum decrease in Schmidt hammer rebound values of 18% below dry rebound values. In porous rocks with high permeability, the Schmidt hammer impact can result in the movement of water through the rock, dissipating the force of the hammer over a larger area. Alternatively, in rocks with low permeability, the presence of incompressible water in closed pore spaces may increase rebound values (Ballanytne et al., 1989). These sensitivities require a

minimum sample size of between 15 and 30 points, depending on rock type, and higher sample sizes for studies that investigate weathering (Niedzielski et al., 2009).

We employed two strategies for collecting Schmidt hammer data along flow perpendicular transects: 1) collection of multiple Schmidt hammer measurements at a given elevation above the thalweg, repeated at different elevations above the thalweg and 2) single Schmidt hammer measurements every 20 cm along flow perpendicular transects. At each site, we used a Topcon laser total station to survey the channel cross-section, taking measurements every 10 cm across the channel. To collect multiple measurements at a particular elevation above the thalweg, we defined transects at various elevations using the survey data. The lowest elevation transect was selected at the lowest point where bedrock was not covered by water. Additional transects were selected at 0.25 m, 0.5 m, 0.75 m, 1 m, 2 m, and over 2 m (where possible) above the lowest transect. Schmidt hammer measurements were collected along transects on both sides of the channel. Using method 1), Schmidt hammer measurements were collected at 5 cm intervals across a 2.5 m long, stream parallel transect, for a total of 50 measurements along each transect. Using method 2), one Schmidt hammer measurement was collected every 20 cm along the surveyed channel cross-section. In order to minimize variability associated with surface roughness not related to the rock surface, lichen, moss, and dirt were carefully removed with a grinding stone, chisel, and paint brush prior to Schmidt hammer measurement. None of the sample sites were characterized by widespread fracturing. Given the large sample sizes, lower Q-values associated with occasional fractures did not significantly alter sample averages.

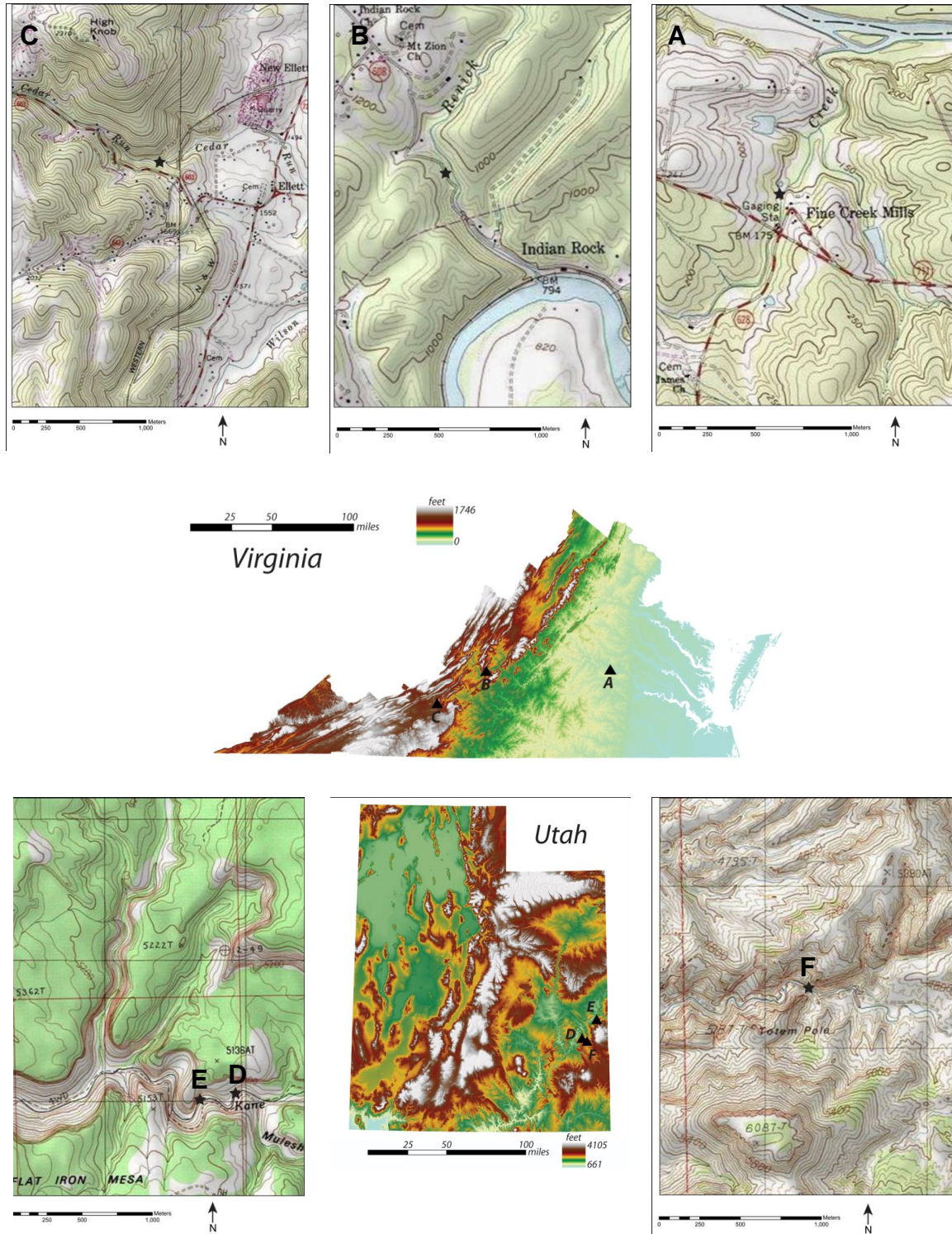


Figure 2: Shaded relief maps with sample site locations identified by letters, which correspond to topographic maps. (A) is Fine Creek, at Fine Creek Mills ~ 20 miles west of Richmond, VA; (B) is Renick Run, near Natural Bridge, VA; (C) is Cedar Run, near Blacksburg, VA; (D) and (E) are Kane Creek, south of Moab, UT; and (F) is Onion Creek, northeast of Moab, UT.

Field Sites

We present data from five different channels from a total of six different sample sites (Figure 2). Sites were chosen primarily based on extent of bedrock exposure, rock type, and ease of access. Channels with full bedrock exposure to ~ 3 meters above the channel bottom on either side were preferred (Figure 3). Three channels were selected in Virginia, which has a humid, temperate climate and an annual average of ~ 40 inches of rain and ~ 15 inches of snow (Table 1). Fine Creek (site A) flows over the Neoproterozoic Fine Creek Mills granitic pluton; a coarse-grained, homogenous granite, with dominant mineralogy of quartz, k-feldspar, plagioclase, and biotite. Renick Run (site B) and Cedar Run (site C) flow over dolomite, limestone, and chert of the Ordovician Beekmantown Formation. Two channels were selected in Utah, which has an arid, desert climate and an annual average of ~ 10 inches of rain and ~ 10 inches of snow (Table 1). Kane Creek (sites D, E) flows over the lower member of the Triassic Moenkopi formation, which is characterized by thinly bedded, fine grained, mudstones and shaly sandstones. Onion Creek (site F) flows over the Permian Cutler formation, composed of thick, arkosic sandstones. Reach averaged slopes were calculated from USGS 7.5' topographic quadrangles, while local slopes were either surveyed in the field or calculated from topographic quadrangles. All streams are perennial but the drainage basins for the Virginia channels are, on average, smaller than those for the Utah channels. Fine Creek receives a consistent low flow due to its well forested drainage basin with low relief. The small drainage basins of Renick Run and Cedar Run provide them with frequent flashy flows. Onion Creek is spring fed and Kane Creek drains the La Sal Mountains.

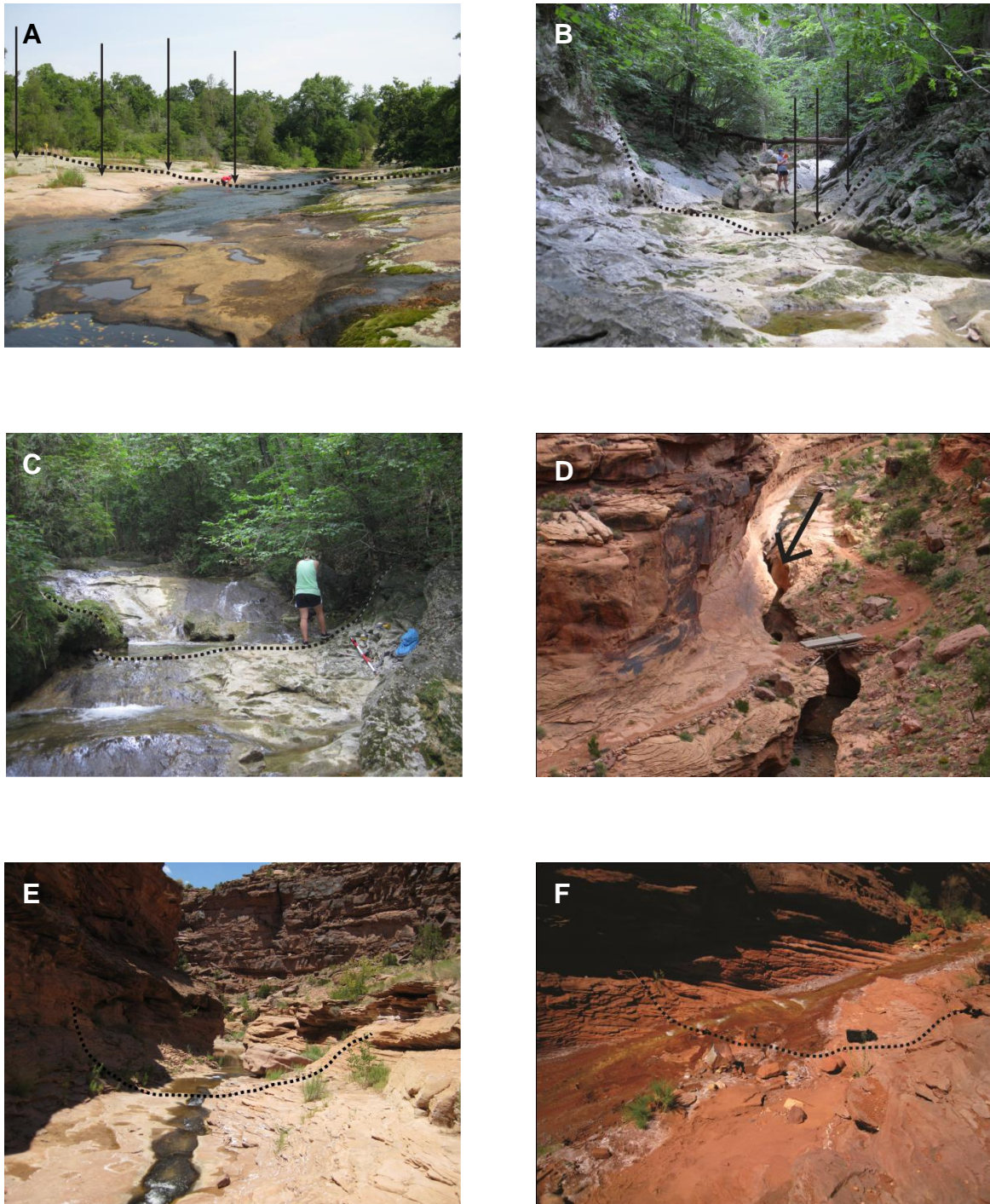


Figure 3: Sample sites with cross sectional survey transect marked. (A) is Fine Creek, VA; (B) is Renick Run, VA; (C) is Cedar Run, VA; (D) slot canyon, Kane Creek, UT; (E) Kane Creek, UT; (F) Onion Creek, UT. Vertical arrows in (A) and (B) indicate location of cores collected to make thin sections for geochemical analysis.

Table 1: Sample site characteristics

Virginia Channels	Rock Type	Upstream Drainage Area (km²)	Reach Averaged Slope / Local Slope
A) Fine Creek	Granite; Proterozoic	65.1	0.010 / 0.008
B) Renick Run	Limestone, dolomite; Ordovician	14.1	0.050 / 0.030
C) Cedar Run	Limestone, dolomite; Ordovician	6.4	0.060 / 0.180
Utah Channels	Rock Type	Upstream Drainage Area (km²)	Reach Averaged Slope / Local Slope
D) Slot Canyon, Kane Creek	Sandstone, mudstone; Triassic	199.2	0.100 / 0.100
E) Kane Creek	Sandstone, mudstone; Triassic	199.1	0.020 / 0.030
F) Onion Creek	Arkosic sandstone; Permian	47.1	0.020 / 0.020

Estimating Flow Frequency

We estimate flow frequency in order to predict the inundation history of bedrock at different elevations above the thalweg. We use USGS stream gage data (only available for site A) and, where gages are not available (all other Virginia and Utah locations), regression equations derived from gauged streams with similar characteristics, in order to calculate discharges associated with the 2 yr, 5 yr, 10 yr, 25 yr, 50 yr, 100 yr, and 500 yr peak floods for each stream. The regression equation used for Virginia channels (sites B and C) scales with drainage basin area (Bisese, 1995) and the regression equation used for two of the three Utah channels (sites E and F) scales with both drainage basin area and average drainage basin elevation (Kenney et al., 2008). Peak flow discharges were not predicted for the slot canyon on Kane Creek (site D), because the flow heights corresponding to all discharges predicted for this channel would be well above the surveyed cross section and any Schmidt hammer point elevations. We use Manning's equation (2) to calculate discharges at 10 cm elevation intervals above the thalweg for each channel:

$$Q = R^{0.67} S^{0.5} A n^{-1} \quad (2)$$

where Q = discharge (m^3s^{-1}), R = hydraulic radius (m), S = local channel gradient, A = channel cross-sectional area (m^2), and n = Manning's roughness coefficient. Channel geometry metrics (R and A) are obtained from cross-sectional survey data. We assume Manning's roughness coefficients between $n = 0.03$ (clean channels) and 0.04 (increased vegetation and boulders in bed; Heritage et al., 2004). We pair peak flow discharge values with discharge values calculated from equation (2) to get a relative idea of the flow depths associated with various peak flows. Standard error of prediction for Virginia

channels is 33 - 60%, which can shift the predicted flow depths for peak floods by (+/-) 0.1 m to 1.0 m. Standard error of prediction for Utah channels is 60 – 108%, which can shift the predicted flow depths for peak flows by (+/-) 0.6 m to 1.4 m

Estimating Weathering Extent

Elemental Analysis and Chemical Weathering Indices

We use electron microprobe mass spectrometry to conduct non-destructive analyses of mineral weathering on a microscopic scale. Elemental data is collected at multiple depths below the rock surface and is used to infer changes in minerals associated with weathering over time. Thin sections (20 μm thick) were prepared from 1 inch diameter rock cores, extracted from multiple elevations above the thalweg. At site A, thin sections were prepared from cores taken at 0 m, 1.1 m, 1.3 m, and 2.9 m above the thalweg along the same cross section where Schmidt hammer measurements were taken. At site B, thin sections were prepared from cores taken at 0.1 m, 0.3 m, and 1.1 m above the thalweg. Additionally, a rock sample was collected from a road cut high above the channel. We assume that this rock has not experienced weathering, so it serves as a baseline for comparison with other samples from this site. At site F, thin sections were prepared from cores taken at 0 m, 0.5 m, 1.0 m, and 2.0 m above the thalweg. All thin sections preserve the exposed rock surface and extend 3 – 6 cm beneath the rock surface. Prior to preparation for the microprobe, point count analyses were conducted on each thin section (500 points), using an Olympus petrographic microscope, in order to verify rock type through identification of dominant mineralogy. X-ray intensity maps and BSE images were acquired for each thin section, using a Cameca Sx100 EPMA at Old Dominion University, equipped with five WDS and operating at a probe current of

58.565 nÅ and an accelerating voltage of 15 keV. $K\alpha$ (Si, Fe, Ca, Na, Ti) peak intensities were collected using large TAP, PET, and LiF monochromator crystals, with a dwell time of 3 s, which allowed for quantitative peak analysis. Peak intensities for Mg, Al, K, and S were collected with EDS using a longer dwell time (8 ms). WDS and EDS were run simultaneously to reduce the total acquisition time. X-ray intensity maps were produced with stage rastering using a stationary beam and a spatial resolution of 5 $\mu\text{m}/\text{pixel}$ over an area of 1024 by 1458 pixels ($\sim 5.1 \text{ mm} \times 7.3 \text{ mm}$), which included the rock surface.

We make a semi-quantitative assessment of weathering by assessing changes in elemental abundances at depth below the surface and through comparison of thin sections taken from different heights within a given channel cross section. Elemental abundances are reported as the elemental weight percent of a common elemental oxide (SiO_2 , Fe_2O_3 , CaO , Na_2O , TiO_2 , MgO , Al_2O_3 , K_2O , SO_2), calculated as the percent of a given elemental oxide of the total elemental oxides present in the solid material in a given row. We compare values of elemental oxides and ratios of mobile elemental oxides to immobile elemental oxides to determine how weathering changes with depth at a particular location. The chemical weathering indices (e.g. Weathering Index of Parker, Chemical Index of Weathering) quantify the transformation of bedrock to soil in transport-limited systems by measuring the degree of depletion of mobile to immobile components during weathering (Price and Velbel, 2003). These indices are based on the principle of isovolumetric weathering, which assumes that elements are removed without a change in rock volume, such that a given volume of weathered rock evolves from an equal volume of fresh rock (Gardner et al., 1978). For each sample site, we calculate weathering indices, based on which elements are most abundant in a given rock sample. Each

weathering index is based on different elemental ratios and different assumptions about elemental mobility. The Weathering Index of Parker (WIP) is applicable for acid, intermediate, or basic silicate rocks where hydrolysis is the main agent of weathering (Parker, 1970):

$$[(2Na_2O*0.35^{-1}) + (MgO*0.9^{-1}) + (2K_2O*0.25^{-1}) + (CaO*0.7^{-1})] * 100 \quad (3)$$

The WIP assumes aluminum mobility, and values over 100 are attributed to fresh rock.

The Ruxton Ratio is a simple weathering index, ideal for humid regions where the composition of the parent rock is known (Ruxton, 1968). It assumes aluminum immobility and the loss of silica with increased weathering:

$$SiO_2*(Al_2O_3)^{-1} \quad (4)$$

where values over 10 are attributed to fresh rock.

The Chemical Index of Alteration essentially measures the extent of conversion of feldspars to clays, and is best applied to silicate rocks with high feldspar content. It assumes aluminum immobility and an increase in alumina to alkali ratio with increased weathering (Nesbitt and Young, 1982):

$$[Al_2O_3*(Al_2O_3 + CaO + Na_2O + K_2O)^{-1}] * 100 \quad (5)$$

where values under 50 are attributed to fresh rock.

The above weathering indices are limited by their inability to account for the addition of elements into the system in question. For spring-fed streams, especially in arid regions, these chemical weathering indices may not adequately describe the extent of rock weathering, since the precipitation of salts may increase elemental concentrations, thus altering weathering indices.

Porosity as a Weathering Index

By assuming isovolumetric weathering, we are able to use percent porosity as another indication of chemical weathering. As isovolumetric weathering progresses through time, the bulk density of the rock sample decreases, such that bulk density can be used as a measure of weathering extent (Price and Velbel, 2003). In order for bulk density to decrease while rock volume stays constant, rock mass must decrease, which is reflected in increasing porosity. Percent porosity is calculated semi-quantitatively for each pixel in the elemental maps according to the elemental differences between measured and theoretical sums of the total oxide weight percentages (Pret et al., 2010). When the sum of total oxide weight percentages was over 100%, percent porosity is assumed to be 0%.

Results

Schmidt Hammer Data

The number of Schmidt hammer measurements varies between sample sites, based on the sampling method used. All Virginia sites were sampled as described in method (1) and all Utah sites were sampled as described in method (2). The Schmidt hammer does not record measurements with Q-values below 13.5, but these data remain important in identifying rock compressive strength. Measurements that fall below this detection limit are given a value of $Q = 10$, a conservative estimate for rocks that may be much weaker, and are included in mean calculations for each elevation bin (red circles, Figure 4). Total number of Schmidt hammer measurements and total number of measurements that fell below the Schmidt hammer detection limit are listed in Table 2. Data are compiled into box and whisker plots for each study site (Figure 4). Mean Schmidt hammer values including measurements below the detection limit and mean Schmidt hammer values not including measurements below the detection limit are graphed for comparison.

Mean Schmidt hammer values (not including points below the detection limit) are significantly different (p -value less than 0.05, using an independent samples t-test) between the lowest elevation bin and the highest elevation bin in five (A, B, C, E, F) of six sample sites. Mean Schmidt hammer values at four (A, C, E, F) of six sites decrease 24 – 52% between the lowest and highest elevations bins, where the highest elevation bin ranges between 1.6 – 3.2 m above channel thalweg. In the Virginia granite, site A, mean Schmidt hammer value decreases by 48% between the waterline and 2 m above the

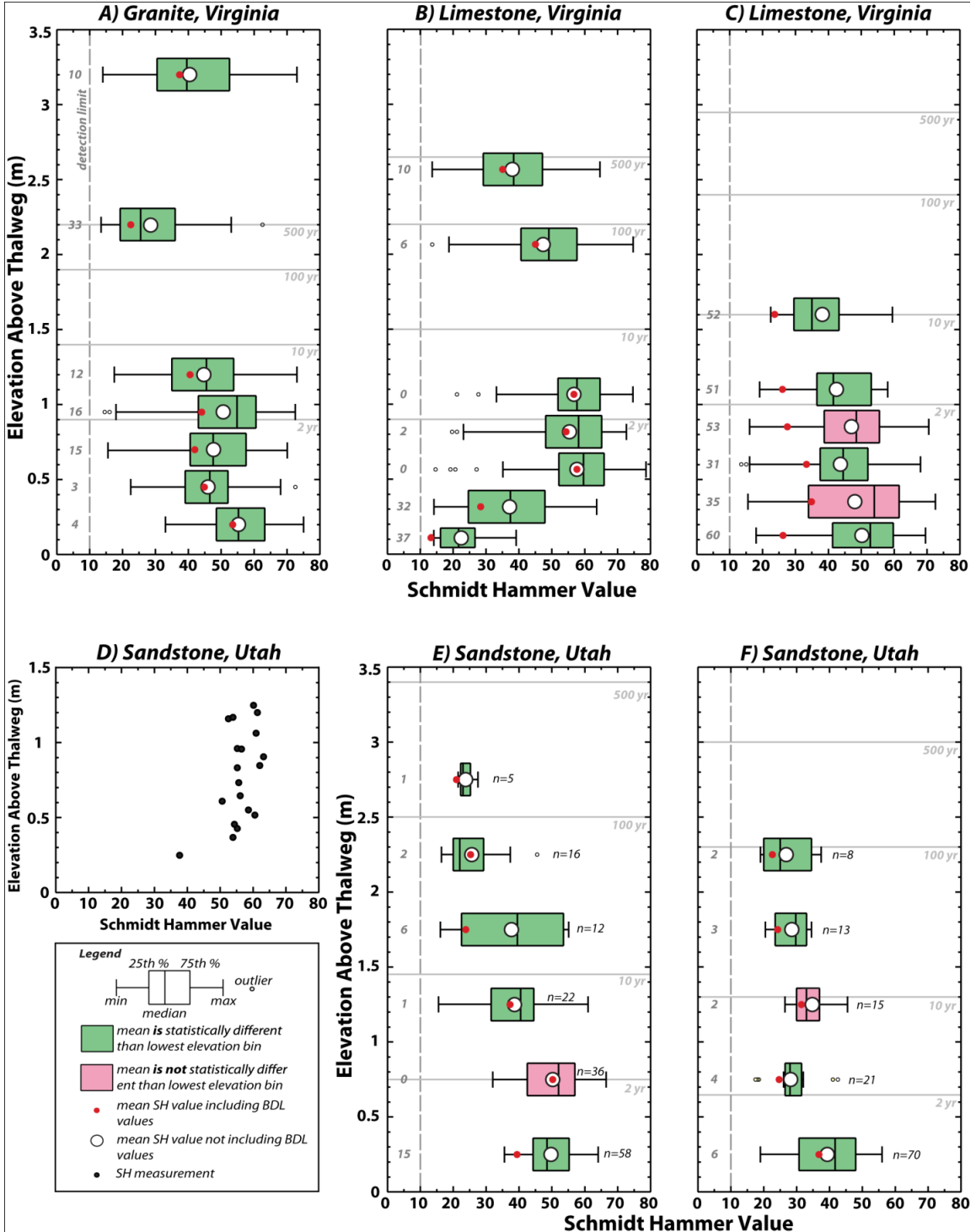


Figure 4: Schmidt hammer value vs. elevation above thalweg. Light gray lines represent peak floods of different recurrence intervals (see text). A total of 19 Schmidt hammer measurements were collected at site (D), which is a rapidly eroding slot canyon located ~ 0.5 km downstream from site (F). Elevation bins in sites (E) and (F) are based on the average of all data points (n-value) that fall within a 0.5 m elevation range, and are plotted at the mid-point of each range.

Table 2: Schmidt hammer data by channel site

Channel Site	Number of Schmidt hammer measurements	
	Total	Below detection limit
Fine Creek	700	92
Renick Run	700	87
Cedar Run	700	282
Slot Canyon, Kane Creek	19	0
Kane Creek	127	17
Onion Creek	149	25

waterline, while the overall decrease in mean Schmidt hammer value at this site is 27%. The smallest decrease occurs at one of the two limestone channels, site C, where mean Schmidt hammer value decreases by 24% between the waterline and 1.6 m above the thalweg. The largest decrease occurs at sandstone channel, site E, where mean Schmidt hammer value decreases by 52% between the lowest elevation bin and the highest elevation bin (3.2 m above channel thalweg). A mean Schmidt hammer decrease of 32% occurs between the lowest elevation bin and the highest elevation bin (1.75 m above channel thalweg) at Utah sandstone, site F.

Mean Schmidt hammer values in two (B, D) of six channels increase 8 – 70% between the waterline and the highest exposed bedrock (1.25 – 2.6 m above thalweg). Mean Schmidt hammer value increases by 8% at the slot canyon on Kane Creek (site D), but this is not a statistically significant increase. At Virginia limestone, site B, an initial increase of 159% occurs between the waterline and 0.6 m above the waterline. Above this elevation, a decrease of 34% occurs between 0.6 m above the thalweg and 2.6 m above the thalweg. The overall change in mean Schmidt hammer value is an increase of 70%.

Mean Schmidt hammer values including points below the detection limit are up to 92% lower than mean Schmidt hammer values without points below the detection limit. The difference in mean Schmidt hammer values is most significant at Virginia limestone, site C, where 282 of 700 measurements are below the Schmidt hammer detection limit (40%). When these mean values are considered, the trend in rock strength at this sample site is similar to the trend observed at Virginia limestone, site B. When values below the detection limit are included, mean Schmidt hammer value shows an initial increase of 33% between the lowest elevation bin and 0.35 m above the thalweg. Above this

elevation, mean Schmidt hammer values decrease by 32% between 0.35 m and 1.6 m above the thalweg.

Channel Geometry

Channel geometry is often described using a width-to-depth ratio, rather than by using width alone. In their recent model, Hancock et al. (2011) consider width-to-depth ratios at mean peak discharges between $\sim 3.1 - 4.6$, where larger width-to-depth ratios are related to increasing differences in rock erodibility between the thalweg and channel margin. Using the cross section survey data, we calculate channel width at multiple depths (every 10 cm), from the thalweg to the highest exposed bedrock. For comparison between channels, width and depth measurements for each site are graphed in Figure 5. The granite channel (site A) shows large increases in width as depth increases. Channel width at bankfull flow is inherently difficult to measure in bedrock channels, since they lack the easily identifiable bankfull width common to alluvial channels. All sample sites have different maximum elevations of bedrock exposure, but in order to make some quantitative comparison of width-to-depth ratios between different channels, we refer to a mid-elevation value, which is calculated at 50% of the maximum elevation above the thalweg. Apart from Virginia granite, site A, which has the highest width-to-depth ratio (mid-elevation = 24), the other channels share relatively similar geometry. The slot canyon on Kane Creek (site D) shows very small increases in width as depth increases. Utah sandstone, site D is narrower than all other channels, with a mid-elevation width to depth ratio of 1. Both Virginia limestone channels (sites B and C) show similar increases in width as depth increases. They have mid-elevation width to depth ratios of 5 (site B)

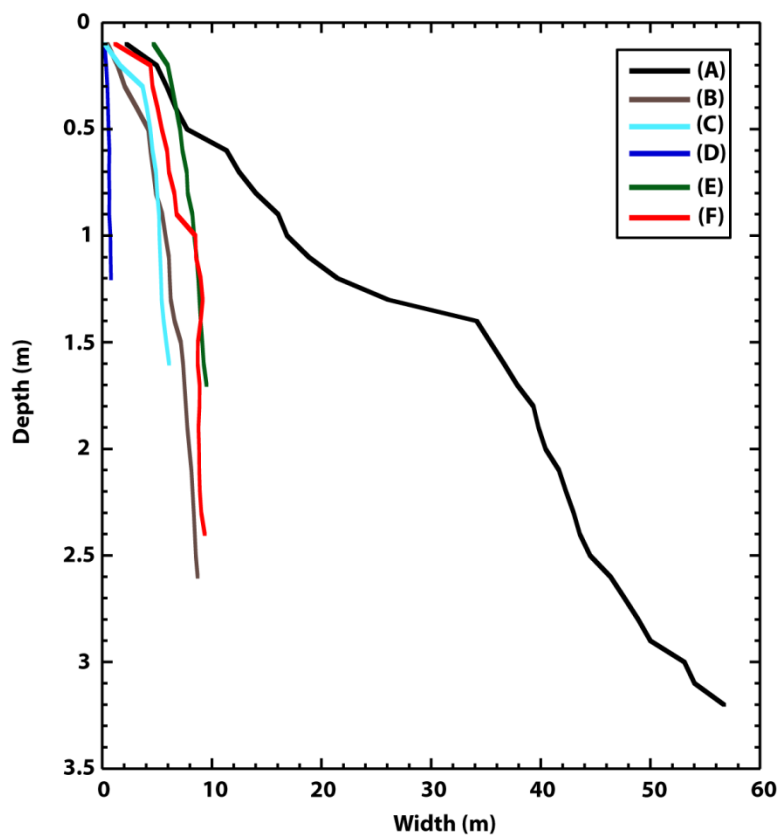


Figure 5: Width vs depth for all channels. Steeper negative slopes indicate narrow channels (e.g., site D), while shallower slopes indicate wide channels (e.g., site A).

and 6.5 (site C). The remaining two Utah sandstone channels (sites E and F) show similar increases in width as depth increase. They have mid-elevation with-to-depth ratios of 9.5 (site E) and 7.5 (site F). The sandstone channels have slightly larger width to depth ratios than both limestone channels.

Microprobe Data

All thin sections were analyzed for weight percent elemental oxides and percent porosity. Different weathering indices are used for each sample site, depending on rock type. The averages for 500 μm sections beneath the surface are plotted for each elemental oxide, weathering index and porosity (Figures 6 – 11).

Virginia Granite, Site A

Plots of weight percent elemental oxides are compiled in Figure 6, and chemical weathering indices and porosity are compiled in Figure 7. The Ruxton Ratio and the Chemical Index of Alteration were calculated for this site, due to the high abundances of silica and aluminum, and for comparison between an index that includes silica and one that does not. All weight percent elemental oxides show variation with increasing depth beneath the surface (Figure 6). Percent porosity is between 5 – 20% for samples 1.1 m, 1.3 m, and 2.9 m, while the 0 m sample is > 40% porous, and up to 95% porous at the surface (Figure 7c). The Ruxton ratio suggests that the surface rock at all elevations is more weathered than rock beneath the surface, and that the upper section of the 0 m sample is more weathered than all other elevations (Figure 7b). The Chemical Index of Alteration, which excludes silica, suggests that the surfaces of the higher elevation samples are more weathered than the surface of the 0 m sample, where the highest two samples are more weathered than both lower ones (Figure 7a).

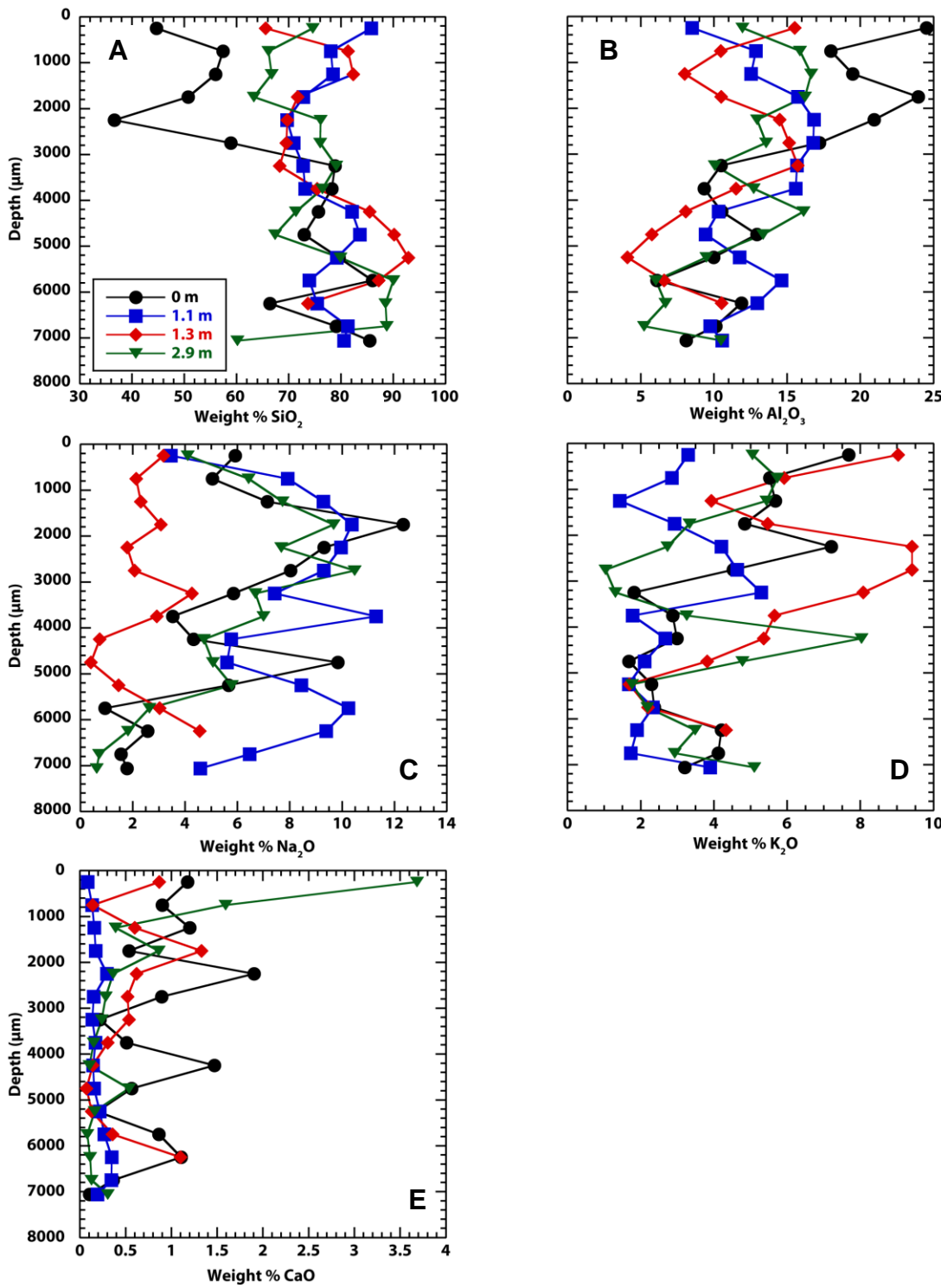


Figure 6: Virginia granite, site A. Weight percent elemental oxides plotted against depth below the surface

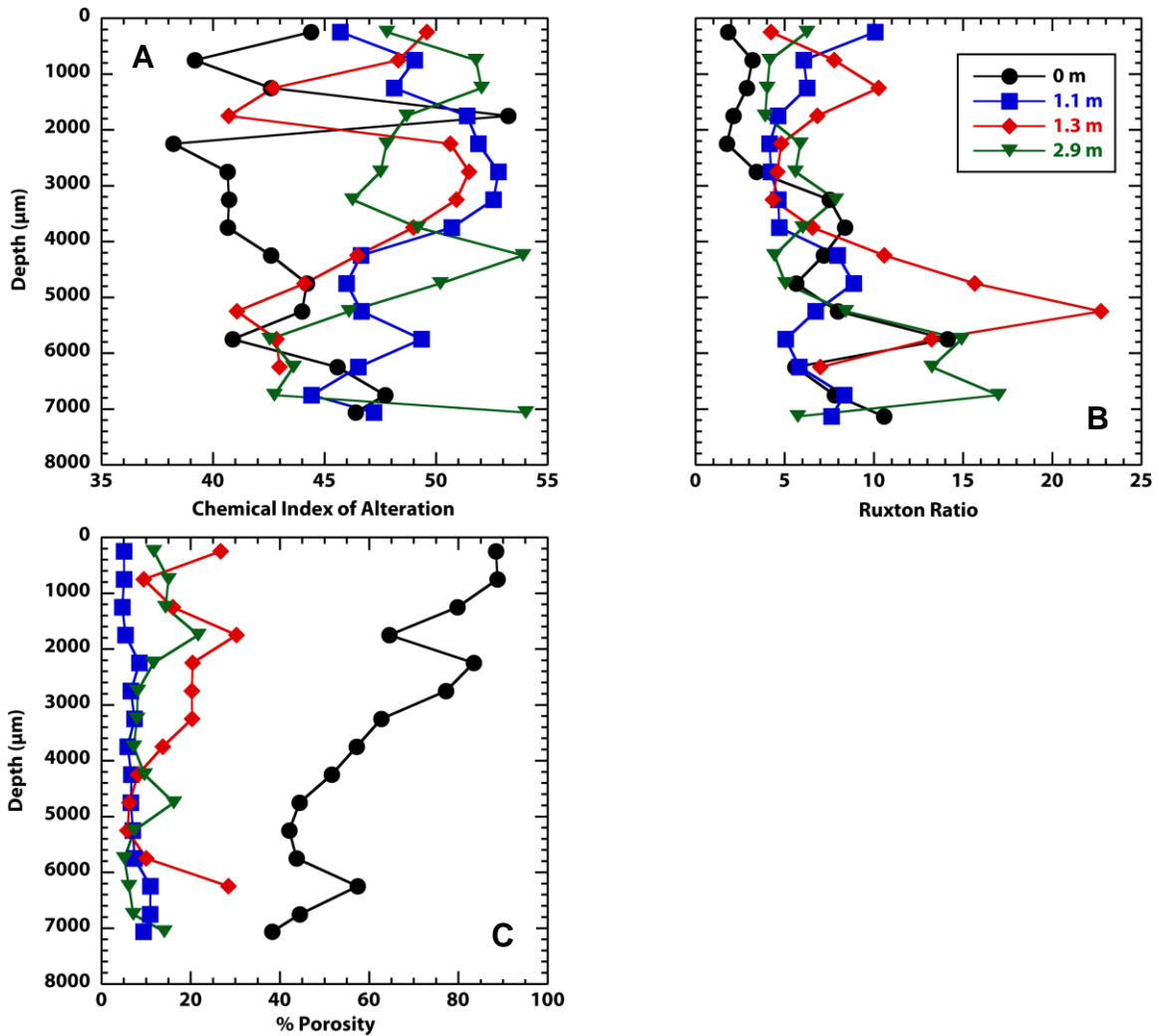


Figure 7: Virginia granite, site A. Chemical weathering indices and percent porosity plotted against depth below the surface. In (A), increasing weathering is indicated by larger numbers. In (B), increased weathering is indicated by smaller numbers.

Virginia Limestone, Site B

Plots of weight percent elemental oxides are compiled in Figure 8, and chemical weathering indices and porosity are complied in Figure 9. The Chemical Index of Alteration and the Weathering Index of Parker were calculated for this site, since both indices account for calcium.

CaO and SiO₂, together, account for between 55 and 85% of oxides in the four samples taken from this location (Figure 8a, 8b). Weight percent CaO varies between 65% in the fresh rock sample and 55% in the highest elevation sample. Weight percent CaO decreases between the 0.1 m sample and the 1.1 m sample. Additionally, weight percent CaO decreases toward the surface in all samples except in the 0.3 m sample, with the most significant decrease (~6%) observed in the 0.1 m sample (Figure 9c). Percent porosity varies from 46% at the 1 m sample to 55% at the fresh rock sample. The Chemical Index of Alteration and the Weathering Index of Parker suggest that the highest elevation rock and the upper 2 mm of rock at the lowest elevation are more weathered than the other two samples (Figure 9a, 9b).

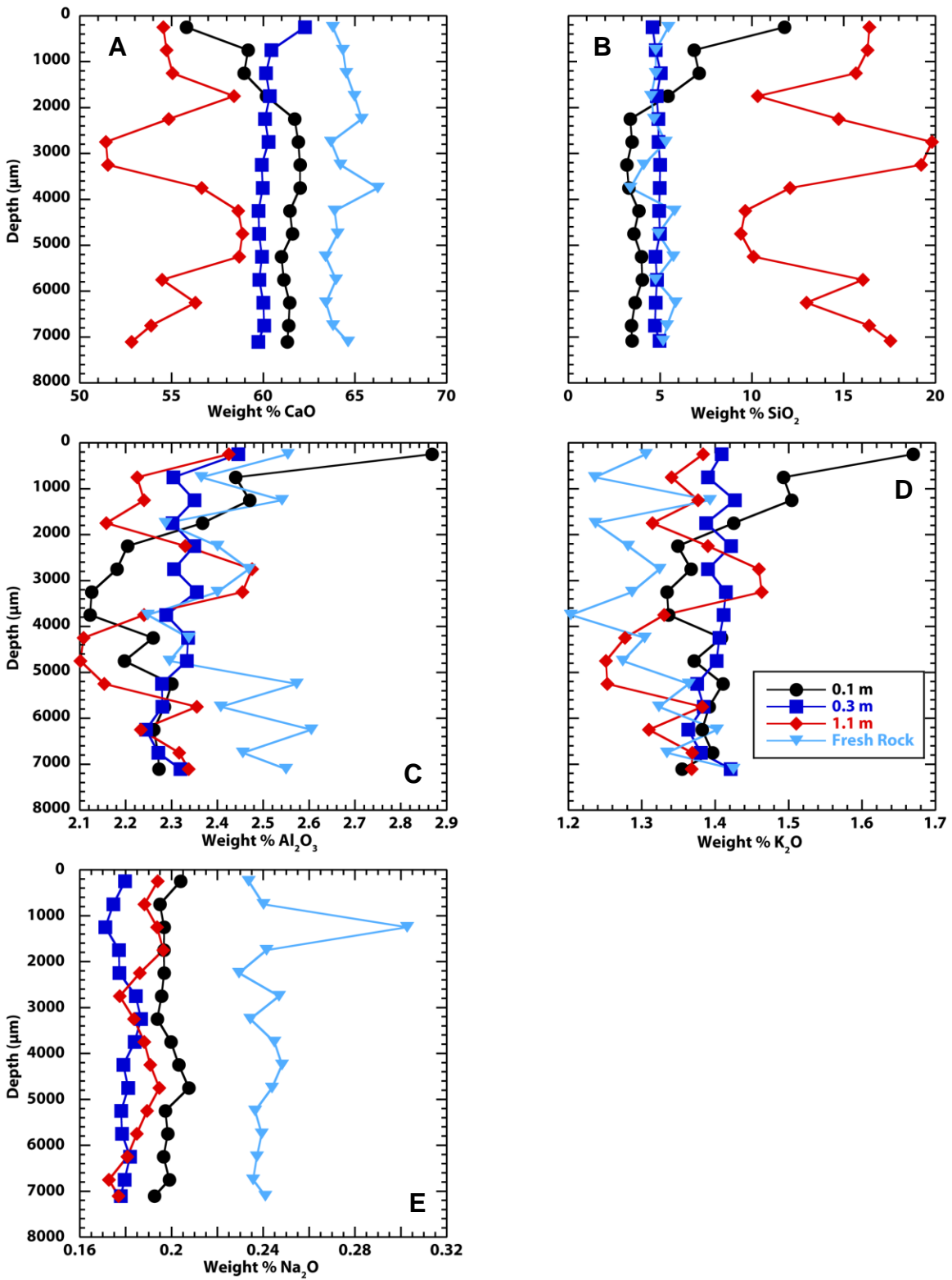


Figure 8: Virginia limestone, site B. Weight percent elemental oxides plotted against depth below the surface.

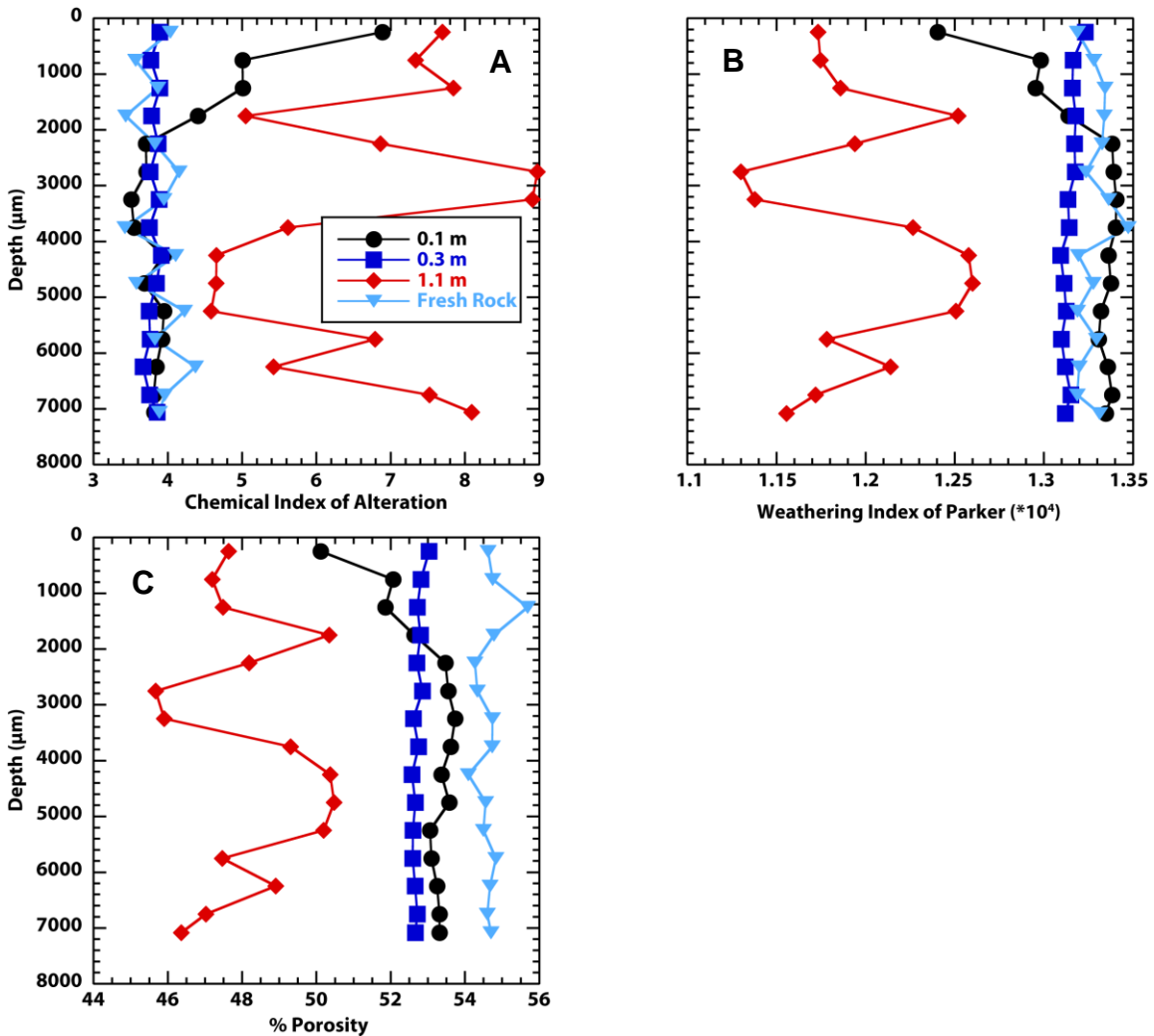


Figure 9: Virginia limestone, site B. Chemical weathering indices and percent porosity plotted against depth below the surface. In (A), increasing weathering is indicated by larger numbers. In (B), increased weathering is indicated by smaller numbers.

Utah Sandstone, Site F

Plots of weight percent elemental oxides are compiled in Figure 10, and chemical weathering indices and porosity are complied in Figure 11. The Ruxton Ratio and the Chemical Index of Alteration were calculated for this site, due to the high abundances of silica, calcium, and aluminum, and for comparison between an index that includes silica and one that does not. Weight percent SiO₂ varies between 50 – 67% of the total oxides in these sandstone samples, where the 2.0 m sample has the lowest percentage and the 0 m sample has the highest percentage (Figure 10a). An equally wide range exists in weight percent CaO, where the 0 m sample has 5% and the 2 m sample has ~ 15% (Figure 10b). Weight percent Al₂O₃ is very similar for all samples at the surface (~ 10%), but it varies significantly with depth, reaching 13% in the 2.0 m sample (Figure 10c). Porosity varies between 20 – 34%, where the lowest porosity is seen in the 0 m sample and the highest percent porosity is seen 5 mm beneath the surface of the 1.0 m sample (Figure 11c). The Chemical Index of Alteration suggests that the 0 m sample is most weathered and the 0.5 m sample is least weathered, while the Ruxton ratio indicates the most weathering in the 2.0 m sample and the least weathering in the 0.5 m sample (Figure 11a, 11b).

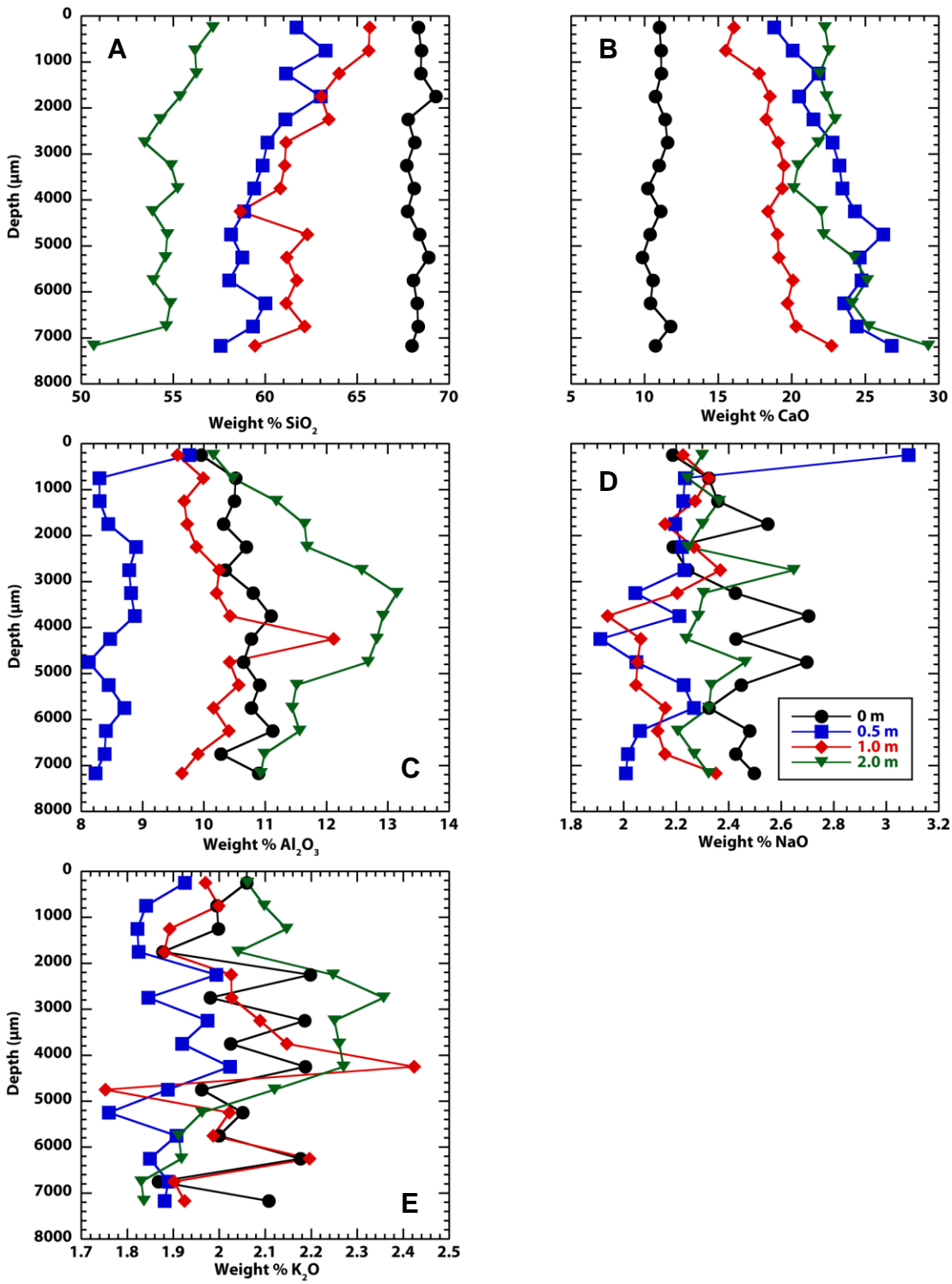


Figure 10: Utah Sandstone, site F. Weight percent elemental oxides plotted against depth below the surface.

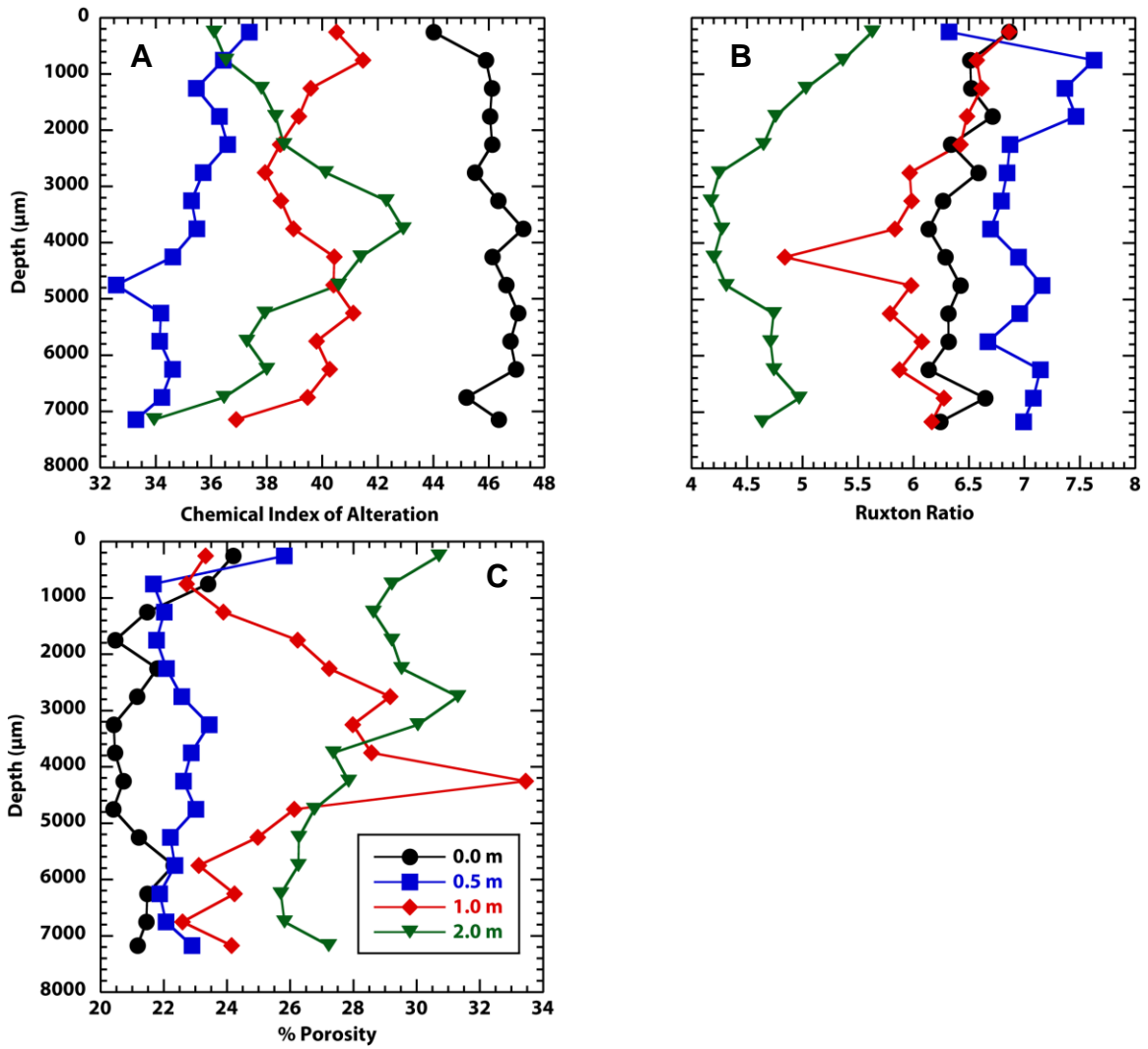


Figure 11: Utah Sandstone, site F. Chemical weathering indices and percent porosity plotted against depth below the surface. In (A), increasing weathering is indicated by larger numbers. In (B), increased weathering is indicated by smaller numbers.

Discussion

Our results indicate that there are significant variations in bedrock chemistry and porosity across many bedrock channels. Porosity and elemental oxide weight percent data suggest variation within bedrock at different elevations above the channel thalweg and at different depths beneath the surface. Variation, although different in each case, is seen across multiple rock types, in both desert and humid climates. The Utah sandstone, site F, shows a systematic increase in porosity with increasing elevation above the thalweg (Figure 11c). Weathering commonly increases porosity, but it can also alter pore distribution, geometry, connectivity, as well as contribute to infilling of original pore space (Sabatakakis, 2008). In sandstone and limestone, increasing percent porosity has been linked to: 1) decreasing uniaxial compressive strength of the rock and 2) lower Schmidt hammer values (Sabatakakis, 2008). These relationships further support the use of the Schmidt hammer as an adequate proxy for rock compressive strength. The higher elevation samples at site F are highly fractured (Figure 12), most likely due to physical weathering by plants, which rapidly exploit freshly exposed fractures (Phillips et al., 2008), and through salt weathering, which is common in spring-fed desert channels (Cooke and Smalley, 1968). Elemental oxide data show that higher elevation samples, all of which are above the 2 yr flow height, have more calcium than the thalweg sample (Figure 10b). The perennial low flow of Onion Creek carries some gypsum ($\text{CaSO}_4 \cdot \text{H}_2\text{O}$) from the Paradox Formation, which outcrops upstream of site F. At high flows, gypsum may be deposited on bedrock at higher elevations, where subsequent thermal expansion and occasional hydration of salt crystals in small fractures may contribute to increasing fracture size (Cooke and Smalley, 1968) and the deposition of calcium. The fractures in

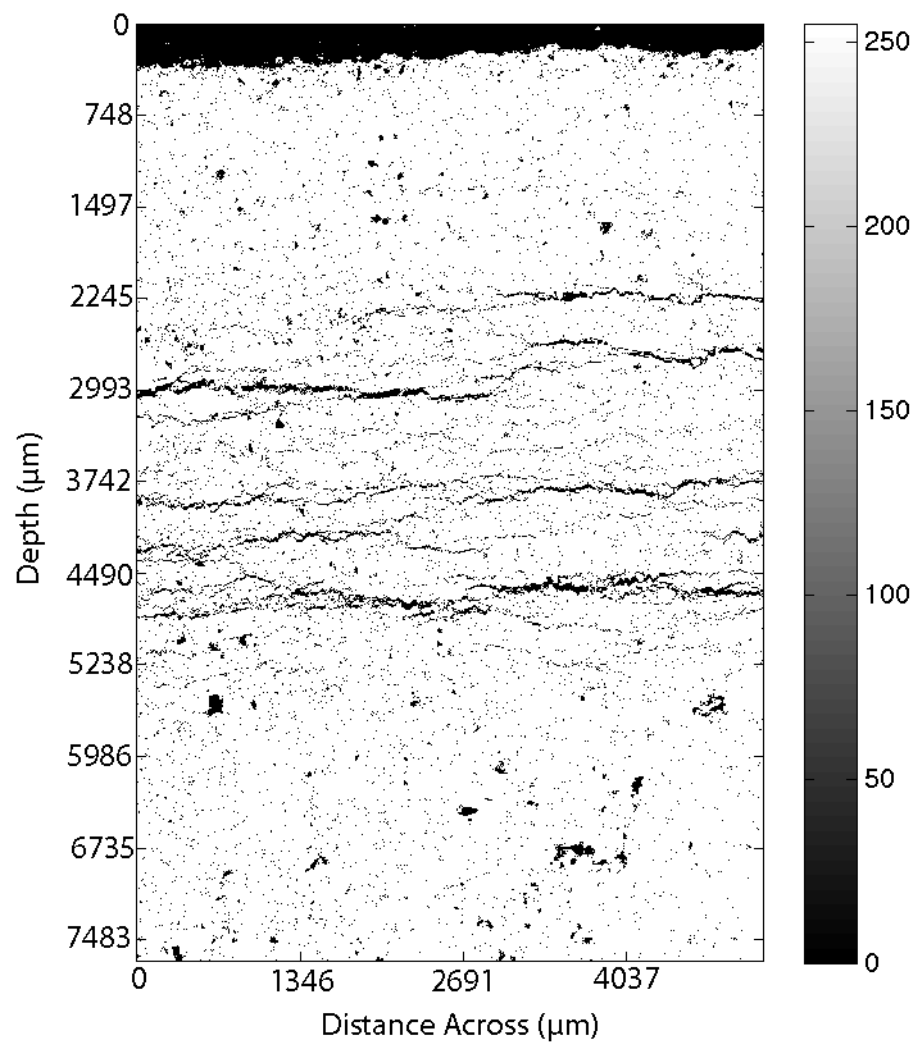


Figure 12: Map of pore space counts for the 1.0 m sample from Utah sandstone, Site F. Black indicates pore space and white indicates rock. Note the horizontal fractures bisecting the thin section at mid-depth.

the 1.0 m sample are concentrated in a zone a few millimeters beneath the surface, suggesting variation on an even smaller scale beneath the bedrock. At site F, samples from each elevation experience a local decrease in porosity within the top 1-2 mm beneath the surface. This may indicate a local zone of increased weathering near the rock surface. The Ruxton ratio, which is the most appropriate weathering index for this site due to the wide range in silica content at different elevations, suggests that the 2.0 m sample is more weathered than lower elevation samples (Figure 11b). The Chemical Index of Alteration (CIA) also indicates greatest weathering in the 2.0 m sample, but all CIA values across all three sample sites are below 50, which would suggest no weathering. While the CIA can be used to describe relative changes in weathering, it appears to be significantly influenced by the addition of elements to the system in consideration, thus it may not be the best index to quantify weathering in bedrock river channels.

In some cases, weathering may also weaken rock at lower elevations. Murphy (2010) observed the formation of saprolite on a point bar upstream (within 0.25 miles) of sample site F. The cover effect, which often limits erosion by shielding the bed from flow (Turowski, 2008b) may cause increased erosion at locations like this, where it may be facilitating weathering by keeping water in contact with underlying bedrock for extended periods of time. Porosity and elemental oxide data were not collected for the Utah sandstones at sites D and E, but the sites are located in the same climate, and similar rock as site F, so we expect similar cross channel differences in weathering exist.

Porosity trends are more ambiguous between different elevations in the Virginia granite, site A (Figure 7c) and the Virginia limestone, site B (Figure 9c). At site A, the

thalweg sample has ~80% porosity, due to abundant fractures throughout, while the higher elevation samples are much less porous, between ~10-20%. Physical weathering through wetting/drying cycles is most efficient in clay rich rocks in hot desert environments, but it can also occur beneath the surface in rocks without abundant clays. In submerged rocks, like the thalweg sample at site A, fluctuations in moisture content may result in fracturing, even without the rock fully drying (Hall and Hall, 1998). Variations in bedrock surface roughness are also observed across site A, ranging from millimeter-scale pitting to smooth, polished rock. Differential weathering of surface grains often creates a textured surface, and is common in heterogeneous rocks (Williams and Robinson, 1983). Site A flows through the heterogeneous Fine Creek Mills granite, which is characterized by large biotite grains, potassium feldspar, and abundant quartz (Figure 13). In crystalline rocks, biotite and feldspars are more susceptible than quartz to weathering through dissolution (Lee et al., 2008). At elevations above the perennial low-flow line, increases in surface roughness can be attributed to weathering through lichen cover, which is abundant in isolated areas throughout the cross section (McCarroll and Nesje, 1996).

At site B, weathering indices indicate extensive weathering in the highest elevation sample (1.1 m) and in the upper millimeter of the thalweg sample (Figure 9a/c). These two samples also have the lowest percent porosity, which may be a result of silica precipitation in pore spaces, as this sample site is situated in and around chert-bearing limestone members of the Beekmantown group (Carroll, 1959). Chert from these rocks may dissolve and move through groundwater as dissolved silica, where it re-crystallizes in pore spaces around topographic lows (e.g. streams) (Carroll, 1959). Both the 1.1 m



Figure 13: Rock core extracted from 0 m at Virginia granite, site A. The surface is to the left. Note fracture 2 cm beneath the surface and heterogeneous nature of the rock. The upper 2 mm is darker than the rest of the rock, which may result from increased weathering near the surface.

sample and upper millimeter of the 0.1 m sample have high % SiO₂, concentrated in irregular shapes in an otherwise calcite dominated limestone (Figure 14). Although these samples have the lowest % porosity, they may be subjected to more weathering than other samples at this site. Dissolution of limestone is common in climates that favor plant growth and non-seasonal precipitation (Simms, 2004). This decrease in CaO in the top millimeter of the 0.1 m is probably associated with increased dissolution in the presence of abundant water (Figure 8a). In this limestone, weathering clearly changes with depth beneath the surface, where the rock closest to the surface weathers significantly more than rock at greater depths. Water was not flowing through site B during sampling, but pools of standing water were present, which facilitates isovolumetric weathering, leading to the formation of the saprolite observed near the channel thalweg (Price and Velbel, 2003) (Figure 15). While there is no data to support any variation seen in bedrock at site C, there were surficial differences in bedrock across the channel. Travertine, a calcium carbonate precipitate, was abundant on only one bank. In order for travertine to precipitate, stream water must become supersaturated with calcium carbonate, usually through increased dissolution associated with the H₂CO₃ produced from the interaction of water with the soil zone or carbonate aquifers (Malusa et al., 2003). In this way, the presence of travertine also indicates increased limestone dissolution. Travertine was not as abundant at site B, but the slight increase in CaO observed at 0.3 m (Figure 8a) may be associated with a ~ 1 mm thick layer of travertine.

While our Schmidt hammer results show variation in rock strength across many channels, they do not always vary systematically with weathering. Compressive strength decreases significantly with increasing elevation at sandstone sites E and F, as well as 17

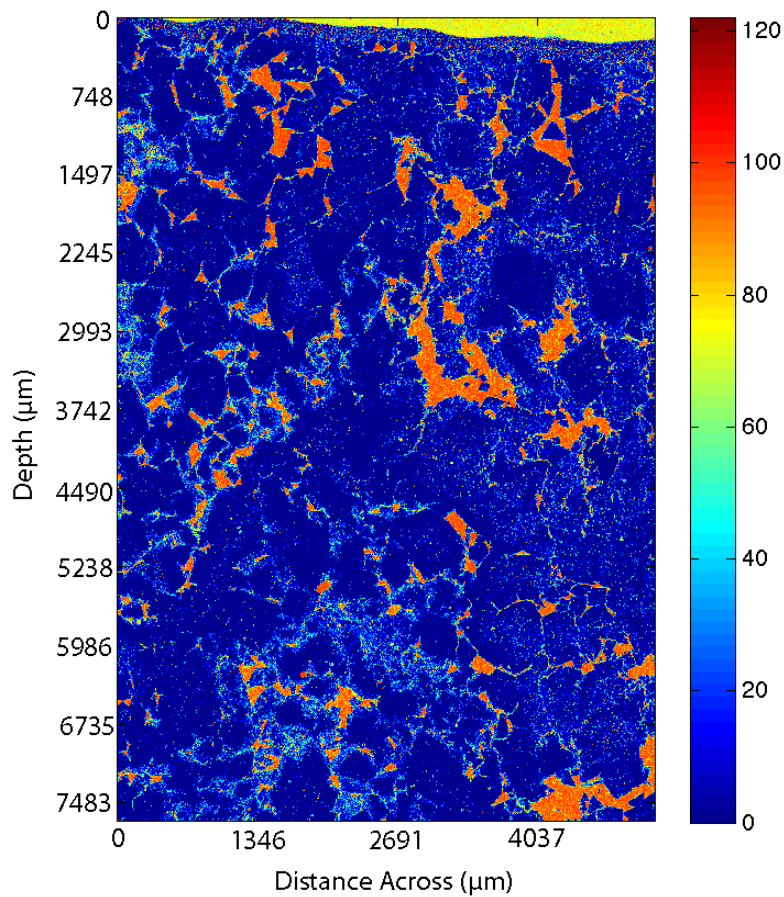


Figure 14: Map of silica distribution for the 1.1 m sample from Virginia limestone, site B. Warm colors (higher counts) indicate more silica. Blue color (low silica counts) is predominantly calcium.



Figure 15: 0.1m transect at Virginia limestone, site B. Dissolution of limestone is forming a saprolite. Note depressions made by the Schmidt hammer plunger, above the measuring tape

sites in Utah sandstone channels (data from Lamp, 2010). In sandstones at sites E and F, the increased weathering at higher elevations suggested by porosity data and the Ruxton Ratio likely contributes to lowering rock strength. These results are similar to those observed by Sklar and Dietrich (2001) in the lab, where weathered samples of granite, limestone, and sandstone were consistently weaker than unweathered samples of the same rock. While a similar trend in decreasing compressive strength with elevation is seen at site A (Figure 4a), our measurements of weathering do not necessarily support the idea that weathering decreases rock strength. Here, porosity data and weathering indices indicate extensive weathering in the thalweg, but the Schmidt hammer data suggests this is the strongest rock across the channel. These results do not discount weathering as a means of increasing rock erodibility, but they suggest that other weathering processes, which we did not measure, are more effective at lowering rock strength at this site.

Schmidt hammer data indicate that compressive strength is most variable in limestone channels (Figure 4b, c). At site B, rock at mid-elevations is strongest, while rock in the thalweg and margins are very weak, with the lowest rock strength concentrated in the thalweg. The increased limestone dissolution and saprolite formation observed at low elevations is contributing to lowering the compressive strength near the thalweg. Our data suggest that bedrock exposed at the highest elevation on the margins is more weathered than rock in the thalweg, but Schmidt hammer data indicate that this rock is slightly stronger than the rock in the thalweg. This may be a result of weathering which is increasing rock strength where the precipitation of elemental oxides (e.g. silica or iron) in pore spaces can serve to strengthen the rock. Above 0.3 m, Schmidt hammer data indicate a steady decline in compressive strength, consistent with increased

weathering suggested by both the Chemical Index of Alteration and the Weathering index of Parker. The bedrock above 0.3 m is not frequently inundated with water, which suggests that physical weathering processes are more effective at these elevations, while chemical dissolution may be more effective in the thalweg.

At sandstone, site D, Schmidt hammer data suggest that bedrock compressive strength is consistent and high at all elevations (Figure 4d). This site, located in a slot canyon, is significantly narrower than all other sample sites (Figure 5) and may be incising faster than all other channels (Turowski et al., 2009). While weathering processes are most effective on rock that is exposed for long periods of time, weathering can still affect rapidly eroding bedrock (Whipple et al., 2000b). Although no changes in compressive strength were observed across site D, differential weathering may occur on a smaller spatial scale than at other channels.

We attribute the variations in compressive strength observed across five of six of these channels, as well as across channels sampled by Murphy (2010) and Lamp (2011), to cross channel differences in weathering. In channels where weathering has decreased bedrock compressive strength, we expect erodibility to increase (Sklar and Dietrich, 2001). In some cases, decreasing compressive strength is most significant on channel margins, rather than the channel center. Modeling by Turowski (2008a) suggests that the cross channel distribution of shear stress leads to greater thalweg erosion during low or moderate flows and erosion of channel margins during floods. Montgomery (2004) and Stock et al. (2005) observed this in the field, where pervasive weathering of sub aerially exposed bedrock on channel margins appeared to be associated with increased erosion rates. Our results suggest that where weathering has weakened bedrock at high

elevations, erodibility may increase more than in the channel center, such that the channel widens faster than it incises (Figure 5a). But, this doesn't necessarily happen in all channels where erodibility is greatest on margins. Both sandstone channels display similar Schmidt hammer data trends to site A, but they also have much lower width-to-depth ratios (Figure 5e/f). This field data provides some validation of scenarios modeled by Hancock et al. (2011). In channels with significant cross channel variations in erodibility, the Hancock et al. (2011) model produces channels with increasing width-to-depth ratios. Data from both limestone channels suggest an additional scenario, not strictly considered in the Hancock et al. (2011) model, where significant cross channel variations in rock strength result in high erodibility in the channel center as well as the channel margins, with lower erodibility at mid elevations. Although erodibility is not constant across the channel, the location of areas of higher erosion may produce a channel geometry similar to that modeled in the low uplift scenario, where the channel maintains its width-to-depth ratio through time.

Results from both field (Stock et al., 2005) and modeling (Turowski et al., 2009) studies have suggested, for various reasons, that stream power based erosion models are too simple to describe erosion seen in natural channels. Our data and results from actual bedrock channels further support the idea that these models may be too simple, as we suggest that weathering, previously ignored in stream power models, may have a significant role in altering the erodibility across bedrock channels.

Conclusion

Our field observations offer support for cross channel variations in the type and extent of bedrock weathering. Variation in weathering was observed between rocks at different elevations above the thalweg. Weathering may also vary at different depths beneath the rock surface. In some of the sandstone and limestone samples, weathering appears to be more extensive in the upper 1-2 mm of bedrock at many different elevations.

Based on previous experiments that have linked rock weathering to rock strength (e.g. Sklar and Dietrich, 2001; Sabatakakis, 2008), we attribute cross channel variations in compressive strength to weathering. In many cases, observed variations appear to be related to the rock elevation above the channel thalweg. Generally, rock strength decreases with increasing height above the thalweg but in some cases, bedrock is very weak in the channel thalweg as well as high on the channel margins, with areas of maximum compressive strength at some mid-elevation.

In many cases, observed variations in rock strength can be linked to variations in erodibility, where decreasing rock strength generally results in increasing rock erodibility. In some cases climate and rock type promote extensive weathering in the channel center, resulting in high bedrock erodibility in the channel center as well as on the channel margins. While weathering does not increase rock erodibility to the same extent at all points in a channel cross section, where it is observed, it contributes to increasing the variability in rock erodibility.

Future Work

Our results have significant implications for landscape evolution models that rely on the shear stress erosion law to model bedrock river erosion. We show that for a given rock type, the erodibility constant, K , is not always constant. More work is required to better constrain the variation in K . This study only considers bedrock in one cross section on each channel. Similar compressive strength measurements should be taken at multiple cross sections at different points along a river in the same rock type in order to establish how much erodibility varies along a river's longitudinal profile. Initial observations suggest that sediment cover can contribute towards significantly altering K by keeping bedrock in contact with water, which facilitates weathering, for extended periods of time. These observations should be investigated with a more quantitative field study.

We also establish that where weathering is active within bedrock channels, it is highly variable. While the geochemical methods utilized in this study have the potential to be more accurate than previous bulk geochemistry methods, they require further refinement. The chemical weathering indices we utilize are designed to describe extensive weathering of bedrock to saprolite. They do not adequately describe the small changes in weathering observed in complex bedrock channels, where elements can potentially be added back into the system. At best, they remain semi-quantitative, and only provide a relative measure of weathering extent within the same rock type. Ideally, they will be corrected so that values for weathering indices can be applied across samples in different channels, in different rock types. In addition to developing geochemical analysis using EPMA, more samples need to be tested from a greater number of different bedrock channels.

Acknowledgements

This research is supported by grants from Ted Dintersmith, the William & Mary Charles Center, and the National Science Foundation Geomorphology and Land Use Dynamics panel (EAR 0922026). I thank Stephen Herman at Old Dominion University facilitating geochemical analyses with the electron probe micro-analyzer. I thank my advisor, Greg Hancock, for invaluable guidance over the past two years. I thank Brendan Murphy for introducing me to bedrock channels, for his guidance as a mentor and friend, and for his stimulating discussions on weathering, erosion, and all things geology related. I thank Lauren Lamp for her dedication as a field assistant and Eric Small and Tevis Blom for assistance during Utah fieldwork in 2010.

References

- Anderson, R.S., 1998. Near-surface thermal profiles in alpine bedrock; implications for the frost weathering of rock. *Arctic and Alpine Research*. 30(4), 362-372.
- Aydin, A., Basu, A., 2005. The Schmidt hammer in rock material characterization. *Engineering Geology*. 81(1), 1-14. doi: 10.1016/j.enggeo.2005.06.006.
- Ballantyne, C.K., Black, N.M., Finlay, D.P., 1990. Use of the Schmidt test hammer to detect enhanced boulder weathering under late-lying snowpatches; reply. *Earth Surface Processes and Landforms*. 15(5), 471-474.
- Berlin, M.M., Anderson, R.S., 2007. Modeling of knickpoint retreat on the Roan Plateau, western Colorado. *Journal of Geophysical Research*. 112(F03S06). doi: 10.1029/2006JF000553.
- Bisese, J.A., 1995. Methods for estimating the magnitude and frequency of peak discharges of rural, unregulated streams in Virginia. *Water-Resources Investigations - U. S. Geological Survey*, 70.
- Bishop, P., Hoey, T.B., Jansen, J.D., Artza, I.L., 2005. Knickpoint recession rate and catchment area; the case of uplifted rivers in eastern Scotland. *Earth Surface Processes and Landforms*. 30(6), 767-778. doi: 10.1002/esp.1191.
- Burbank, D.W., Leland, J., Fielding, E., Anderson, R.S., Brozovic, N., Reid, M.R., Duncan, C., 1996. Bedrock incision, rock uplift and threshold hillslopes in the northwestern Himalayas. *Nature (London)*. 379(6565), 505-510. doi: 10.1038/379505a0.
- Carroll, D., 1959. Sedimentary studies in the Middle River drainage basin of the Shenandoah Valley of Virginia. USGS Professional Paper 314-F. Shorter contributions to general geology. 125-154.
- Cerna, B., Engel, Z., 2011. Surface and sub-surface Schmidt hammer rebound value variation for a granite outcrop. *Earth Surface Processes and Landforms*. 36(2), 170-179. doi: 10.1002/esp.2029.
- Cooke, R.U., Smalley, I.J., 1968. Salt Weathering in Deserts. *Nature*. 220(5173), 1226-1227.
- Day, M.J., 1980. Rock hardness; field assessment and geomorphic importance. *The Professional Geographer*. 32(1), 72-81.
- Day, M.J., Goudie, A.S., 1977. Field assessment of rock hardness using the Schmidt test hammer. *Technical Bulletin - British Geomorphological Research Group*(18), 19-29.

- Duvall, A., Kirby, E., Burbank, D., 2004. Tectonic and lithologic controls on bedrock channel profiles and processes in coastal California. *Journal of Geophysical Research.* 109(F03002). doi: 10.1029/2003JF000086.
- Finnegan, N.J., Sklar, L.S., Fuller, T.K., Anonymous, 2007. Interplay of sediment supply, river incision, and channel morphology revealed by the transient evolution of an experimental bedrock channel. *Journal of Geophysical Research.* 112(F03S11). doi: 10.1029/2006JF000569.
- Foley, M.G., 1980. Bed-rock incision by streams. *Geological Society of America Bulletin.* 91(10), 2189-2213.
- Gardner, L.R., Kheoruenromne, I., Chen, H.S., 1978. Isovolumetric geochemical investigation of a buried granite saprolite near Columbia, SC, U.S.A. *Geochimica et Cosmochimica Acta.* 42(4), 417-424.
- Goudie, A.S., 2006. The Schmidt hammer in geomorphological research. *Progress in Physical Geography.* 30(6), 703-718. doi: 10.1177/0309133306071954.
- Gupta, V., Sharma, R., Sah, M.P., 2011. Surface weathering of gneiss, northwestern higher Himalaya, India. *Quarterly Journal of Engineering Geology and Hydrogeology.* 44(1), 135-140. doi: 10.1144/1470-9236/09-064.
- Hall, K., Hall, A., 1996. Weathering by wetting and drying: Some experimental results. *Earth Surface Processes and Landforms.* 21(4), 365-376.
- Hancock, G.S., Small, E.E., Wobus, C., 2011. Modeling the effects of weathering on bedrock-floored channel geometry. *Journal of Geophysical Research.* 116(F03018).
- Hancock, G.S., Anderson, R.S., Whipple, K.X., 1998. Beyond power; bedrock river incision process and form. *Geophysical Monograph.* 107, 35-60.
- Harnois, L., 1988. The CIW index; a new chemical index of weathering. *Sedimentary Geology.* 55(3-4), 319-322.
- Hartshorn, K., Hovius, N., Dade, W.B., Slingerland, R.L., 2002. Climate-driven bedrock incision in an active mountain belt. *Science.* 297(5589), 2036-2038. doi: 10.1126/science.1075078.
- Heritage, G.L., Moon, B.P., Broadhurst, L.J., James, C.S., 2004. The frictional resistance characteristics of a bedrock-influenced river channel. *Earth Surface Processes and Landforms.* 29(5), 611-627. doi: 10.1002/esp.1057.
- Howard, A.D., Dietrich, W.E., Seidl, M.A., 1994. Modeling fluvial erosion on regional to continental scales. *Journal of Geophysical Research.* 99(B7), 986. doi: 10.1029/94JB00744.

- Howard, A.D., Kerby, G., 1983. Channel changes in badlands. Geological Society of America Bulletin. 94(6), 739-752.
- Katz, O., Reches, Z., Roegiers, J.C., 2000. Evaluation of mechanical rock properties using a Schmidt Hammer. International Journal of Rock Mechanics and Mining Sciences (1997). 37(4), 723-728.
- Kenney, T.A., Wilkowske, C.D., Wright, S.J., 2007. Methods for estimating magnitude and frequency of peak flows for natural streams in Utah. Scientific Investigations Report, 28.
- Lee, S.Y., Kim, S.J., Baik, M.H., 2008. Chemical weathering of granite under acid rainfall environment, Korea. Environmental Geology. 55(4), 853-862.
- Malusa, J., Overby, S.T., Parnell, R.A., 2003. Potential for travertine formation. Applied Geochemistry. 18(7), 1081-1093.
- Matthews, J.A., Winkler, S., 2011. Schmidt-hammer exposure-age dating (SHD): application to early Holocene moraines and a reappraisal of the reliability of terrestrial cosmogenic-nuclide dating (TCND) at Austanbotnbreen, Jotunheimen, Norway. Boreas. 40, 256-270.
- Matthews, J.A., Shakesby, R.A., 1984. The status of the "Little Ice Age" in southern Norway; relative-age dating of Neoglacial moraines with Schmidt hammer and lichenometry. Boreas. 13(3), 333-346.
- McCarroll, D., 1922. A new instrument and techniques for the field measurement of rock surface roughness. Zeitschrift fur Geomorphologie. 39, 69-79.
- McCarroll, D., 1991. The Schmidt hammer, weathering and rock surface roughness. Earth Surface Processes and Landforms. 16(5), 477-480.
- Montgomery, D.R., 2004. Observations on the role of lithology in strath terrace formation and bedrock channel width. American Journal of Science. 304(5), 454-476.
- Montgomery, D.R., Gran, K.B., 2001. Downstream variations in the width of bedrock channels. Water Resources Research. 37(6), 1841-1846. doi: 10.1029/2000WR900393
- Nesbitt, H.W., Young, G.M., 1982. Early Proterozoic climates and plate motions inferred from major element chemistry of lutites. Nature. 299, 715-717. doi: 10.1038/299715a0.
- Niedzielski, T., Migon, P., Placek, A., 2009. A minimum sample size required from Schmidt hammer measurements. Earth Surface Processes and Landforms. 34(13), 1713-1725. doi: 10.1002/esp.1851.

Parker, A., 1970. An Index of Weathering for Silicate Rocks. *Geological Magazine*, 107, 501-504. doi: 10.1017/S0016756800058581.

Phillips, J.D., Turkington, A.V., Marion, D.A., 2008. Weathering and vegetation effects in early stages of soil formation. *Catena (Giessen)*. 72(1), 21-28. doi: 10.1016/j.catena.2007.03.020.

Pret, D., Sammartino, S., Beaufort, D., Fialin, M., Sardini, P., Cosenza, P., Meunier, A., 2010. A new method for semi-quantitative petrography based on image processing of chemical element maps: Part II. Semi-quantitative porosity maps superimposed on mineral maps. *American Mineralogist*, 95, 1389-1398. doi: 10.2138/am.2010.3433.

Price, J.R., Velbel, M.A., 2003. Chemical weathering indices applied to weathering profiles developed on heterogeneous felsic metamorphic parent rocks. Elsevier, Amsterdam, Netherlands, pp. 397-416. doi: 10.1016/j.chemgeo.2002.11.001.

Ruxton, B.P., 1968. Measures of the degree of chemical weathering of rocks. *The Journal of Geology*. 76(5), 518-527.

Sabatakakis, N., Koukis, G., Tsiambaos, G., Papanakli, S., 2008. Index properties and strength variation controlled by microstructure for sedimentary rocks. *Engineering Geology*. 97(1), 80-90.

Seidl, M.A., Dietrich, W.E., 1992. The problem of channel erosion into bedrock. *Catena Supplement*. 23, 101-124.

Selby, M.J., 1980. A rock mass strength classification for geomorphic purposes; with tests from Antarctica and New Zealand. *Zeitschrift fuer Geomorphologie*. 24(1), 31-51.

Simms, M.J., 2004. Tortoises and hares: dissolution, erosion and isostasy in landscape evolution. *Earth Surface Processes and Landforms*. 29(4), 477-494.

Sklar, L.S., Dietrich, W.E., 2001. Sediment and rock strength controls on river incision into bedrock. *Geology (Boulder)*. 29(12), 1087-1090.

Stark, C.P., 2006. A self-regulating model of bedrock river channel geometry. *Geophysical Research Letters*. 33(4), 5. doi: 10.1029/2005GL023193.

Stock, J.D., Montgomery, D.R., Collins, B.D., Dietrich, W.E., Sklar, L.S., 2005. Field measurements of incision rates following bedrock exposure; implications for process controls on the long profiles of valleys cut by rivers and debris flows. *Geological Society of America Bulletin*. 117(1-2), 174-194. doi: 10.1130/B25560.1.

Sumner, P., Nel, W., 2002. The effect of rock moisture on Schmidt hammer rebound; tests on rock samples from Marion Island and South Africa. *Earth Surface Processes and Landforms*. 27(10), 1137-1142. doi: 10.1002/esp.402.

Suzuki, T. and Takahashi, K., 1981. An experimental study of wind abrasion. *The Journal of Geology*. 89(4), 509-522.

Turowski, J.M., Lague, D., Hovius, N., 2009. Response of bedrock channel width to tectonic forcing; insights from a numerical model, theoretical considerations, and comparison with field data. *Journal of Geophysical Research*. 114(F03016). doi: 10.1029/2008JF001133.

Turowski, J.M., Hovius, N., Meng-Long, H., Lague, D., Men-Chiang, C., 2008a. Distribution of erosion across bedrock channels. *Earth Surface Processes and Landforms*. 33, 353-363. doi: 10.1002/esp.1559.

Turowski, J.M., Hovius, N., Wilson, A., Horng, M.J., 2008b. Hydraulic geometry, river sediment and the definition of bedrock channels. *Geomorphology*. 99(1-4), 26-38. doi: 10.1016/j.geomorph.2007.10.001.

Whipple, K.X., 2004. Bedrock rivers and the geomorphology of active orogens. *Annual Review of Earth and Planetary Sciences*. 32, 151-185. doi: 10.1146/annurev.earth.32.101802.120356.

Whipple, K.X., 2001. Fluvial landscape response time; how plausible is steady-state denudation?. *American Journal of Science*. 301(4-5), 313-325.

Whipple, K.X., Snyder, N.P., Dollenmayer, K., 2000b. Rates and processes of bedrock incision by the Upper Ukak River since the 1912 Novarupta ash flow in the Valley of Ten Thousand Smokes, Alaska. *Geology*. 28(9), 835-838.

Whipple, K.X., Tucker, G.E., 1999. Dynamics of the stream-power river incision model; implications for height limits of mountain ranges, landscape response timescales, and research needs. *Journal of Geophysical Research*. 104(B8), 674. doi: 10.1029/1999JB900120.

Williams, R.B.G., Robinson, D.A., 1983. The effect of surface texture on the determination of the surface hardness of rock using the Schmidt hammer. *Earth Surface Processes and Landforms*. 8(3), 289-292.

Wobus, C.W., Tucker, G.E., Anderson, R.S., 2006. Self-formed bedrock channels. *Geophysical Research Letters*. 33(18). doi: 10.1029/2006GL027182.

Appendix A: Transect Survey, Schmidt Hammer, and Channel Geometry Data.

Survey Data		Site A			
Distance Across Channel (m)	Elevation Above Thalweg (m)	10.97	1.12	23.97	0.52
0.00	3.61	11.24	1.10	24.23	0.54
0.29	3.60	11.46	1.10	24.41	0.53
0.52	3.53	11.68	1.08	24.68	0.47
0.75	3.46	11.94	1.07	24.77	0.37
0.81	3.26	12.13	1.04	25.05	0.33
0.98	3.12	12.39	1.01	25.27	0.34
1.02	2.85	12.59	0.95	25.52	0.35
1.22	2.69	12.85	0.90	25.76	0.36
1.40	2.59	12.99	0.86	25.94	0.43
1.64	2.55	13.30	0.83	26.17	0.52
1.82	2.43	13.49	0.81	26.42	0.58
2.07	2.31	13.76	0.80	26.61	0.58
2.19	2.08	13.96	0.77	26.88	0.67
2.47	2.02	14.24	0.76	27.09	0.71
2.70	2.01	14.44	0.71	27.36	0.76
2.85	2.03	14.66	0.69	27.52	0.77
3.11	1.95	14.90	0.66	27.85	0.82
3.30	1.91	15.17	0.62	28.07	0.84
3.41	1.70	15.37	0.59	28.31	0.84
3.76	1.58	15.63	0.56	28.48	0.83
4.01	1.51	15.87	0.52	28.78	0.88
4.30	1.42	16.11	0.48	29.02	0.92
4.46	1.42	16.33	0.43	29.25	0.99
4.59	1.40	16.58	0.41	29.51	1.02
4.79	1.40	16.79	0.36	29.76	1.04
5.06	1.38	17.04	0.31	29.96	1.06
5.20	1.36	17.24	0.23	30.25	1.09
5.45	1.35	17.50	0.24	30.50	1.12
5.62	1.34	17.74	0.20	30.74	1.14
5.91	1.32	17.92	0.19	30.89	1.14
6.08	1.30	18.21	0.19	31.21	1.16
6.35	1.29	18.47	0.18	31.44	1.17
6.59	1.29	18.70	0.16	31.69	1.21
6.86	1.29	18.96	0.14	31.93	1.22
7.06	1.27	19.21	0.13	32.17	1.29
7.33	1.28	19.46	0.15	32.41	1.32
7.55	1.28	19.70	0.14	32.67	1.34
7.77	1.27	19.95	0.13	32.87	1.34
7.94	1.27	20.18	0.04	33.17	1.33
8.18	1.24	20.39	0.00	33.41	1.33
8.42	1.22	20.62	0.01	33.67	1.30
8.74	1.22	20.84	0.04	33.87	1.27
8.96	1.18	21.13	0.07	34.12	1.24
9.23	1.21	21.40	0.06	34.37	1.21
9.42	1.20	21.63	0.05	34.62	1.19
9.68	1.21	21.88	0.06	34.85	1.15
9.87	1.21	22.12	0.09	35.10	1.13
10.12	1.21	22.39	0.12	35.30	1.07
10.27	1.17	22.58	0.16	35.59	1.00
10.56	1.15	22.82	0.26	35.80	0.92
10.77	1.13	23.04	0.34	36.01	0.81
		23.28	0.39	36.21	0.80
		23.51	0.45	36.45	0.79
		23.75	0.50	36.71	0.83
				49.38	2.73
				49.57	2.74
				49.83	2.75
				50.00	2.80
				50.28	2.84
				50.45	2.86
				50.71	2.88
				50.89	2.90
				51.16	2.91
				51.35	2.92
				51.60	2.93
				51.80	2.94
				52.05	2.95
				52.34	2.96
				52.51	2.96
				52.76	2.96
				52.99	2.96
				53.23	2.95
				53.66	2.94
				53.93	2.95
				54.18	3.02
				54.42	3.06
				54.62	3.07
				54.74	3.07
				54.87	3.09
				55.09	3.11
				55.34	3.11
				55.59	3.12
				55.81	3.12
				56.02	3.13
				56.30	3.13
				56.53	3.14
				56.75	3.15
				56.99	3.16
				57.25	3.18
				57.48	3.19
				57.76	3.21

Schmidt Hammer Q-Value, Elevation Above Thalweg (m)						
0.20 m	0.45 m	0.70 m	0.95 m	1.2 m	2.2 m	3.2 m
45	47.5	29.5	59.5	28	25.5	
50	49.5	35.5		42	18.5	
48	55		47	42.5	25	14.5
51.5	59	32.5	24.5	19.5	16.5	
54.5	28.5	40.5	59.5	68.5	18	17
	48	42	65.5	22		18
54	46.5		60.5	41.5	26.5	24
37.5	50	32	64	44.5	22	18
55	46.5	63	44.5	61.5		17.5
38	55.5		36	55	25	
56	44	35		73		14
59.5	46.5		23	51	15.5	16
58	56		37.5	51		22
48	58	19	57	53	14	20
47.5	56.5	58	39.5	41.5		
41	44.5		48.5	58		
43	37	45	55	50.5	14.5	25
47.5		49.5	49	58.5		30.5
40	42	56	46	38		21.5
49.5	61.5	52.5	55	33.5		20.5
52	38.5	26.5		62	14.5	31
66	27	30		24.5		32
52	47	40	56	52	18	35.5
58	35.5	41	36	56	25	40
58.5	56				21.5	31
51.5	28.5	63	49	49		
66	60	64	52	30	14	40.5
47.5	50.5	23.5	42.5	57.5	21	33.5
48	45	63.5	52.5	30		42.5
58.5	55	42	59.5	53	13.5	37.5
46	36.5	56	43.5	68	16	32.5
48	58	57.5		59.5	14.5	41.5
50	31.5	57.5	50.5	52.5	17.5	24
59.5	40.5	62.5	46.5		26	27.5
66	46.5	38.5	52.5	62.5		34.5
55.5	46.5	54.5	31			35.5
50.5	44.5		57	52.5	19.5	34.5
43.5	22.5	43.5	39.5	32	19.5	40.5
52.5	29.5		66	28.5	21	34
49.5	34.5	44	28.5	47	25.5	28.5
56.5	43.5	41.5	44	56.5	26	33
53	24	53.5	18	37	36.5	31.5
58	49	44	20	31.5		33.5
	33.5	42.5		54.5		39
68.5	43	46	23	46.5		25.5
67.5	45.5	48		34		30
66.5	60	42.5				24
45	39.5			17.5	31.5	23.5
49	23	38		25	15.5	39
52	61.5	15.5	30	41.5	23.5	32.5
65.5	68	60			29.5	55.5
33	65.5			28		57.5
66.5	65	45.5	60.5	55	52	
63.5	72.5	59	58.5	40	19	62
55	62.5	41	68.5	46.5	62	33

74	60.5	64	54.5	49.5		40.5
57	44	51.5	60	60.5		24
75			65	35.5	35	46
45.5	28.5	47.5	66.5	42.5	21.5	43
62.5	31	41.5	49		41	66
71	34.5	49.5	63.5	28.5		41
42.5	31	56	60	40.5	18.5	44.5
63.5	28	59.5	60		27.5	43.5
45	41	40.5	68.5		17	48
63.5	39	29.5	44.5	43.5	35.5	46
70.5	34.5	54.5	50.5	36	31	60
49	38	50.5	64.5	41		47.5
47.5	56.5		36	30		26
64.5	50			46.5		43
43.5	52.5	54		36.5	43	37
69	51.5	50.5	57.5	29	30.5	54
56.5	51	41	59			
55	60	64	63.5	20.5	50.5	59
63	45.5	44	69.5	48		62
64	50.5	56	61	53.5		49
59	46.5	32.5	62.5	33		61
59.5	45	48.5	52.5	40.5	50.5	73
	55	65	54.5	30.5	30	51.5
56.5	48	63.5	55.5		45.5	
61	53	54.5	70.5	39	33.5	49
38.5	47.5		67	53.5	24	38
56	50.5	70	59.5	43	40.5	52.5
56.5	52	60	58	51.5	43.5	71.5
58	49.5	25.5	42.5	61.5	37.5	56.5
65.5	50.5	36	25	57	22.5	57.5
	47.5	36	25.5	50.5	34	69.5
54	45	54	14.5		33.5	55
54.5	49	44.5	25		21	61
66	49	60	16	37	37	63
70.5	46	35	58	51		55
63.5	44.5	70	44.5	55.5	42	56.5
66	43	58.5	53	54	35.5	39
58.5	44.5	32.5	60.5	45.5	24.5	32.5
69	44	37	57.5	58	28.5	54.5
52.5	47.5	49	72.5	33	39	63.5
37	45.5	69	67.5	34.5	46	52.5
54	38.5	62	63	42.5		41
56	28.5	46	66.5	45.5	53	44
51	37	47	64.5	51	40.5	47
63		59.5		59		51.5

Channel Geometry						
Elevation Above Thalweg (m)	Width (m)	Width-to-depth ratio	Wetted Perimeter (m)	Cross Sectional Area (m^2)	Hydraulic Radius (m)	Discharge (m^3s^-1)
0.1	2.21	22.06	2.25	0.10	0.00	0.04
0.2	4.95	24.75	5.03	0.48	0.02	0.30
0.3	5.86	19.55	5.95	1.03	0.05	0.97
0.4	6.70	16.74	6.97	1.66	0.10	1.94
0.5	7.76	15.51	8.09	2.39	0.15	3.23
0.6	11.34	18.90	11.71	3.67	0.19	5.15
0.7	12.48	17.82	12.64	4.90	0.27	7.90
0.8	14.02	17.53	14.18	6.25	0.36	10.98
0.9	16.05	17.83	16.37	7.71	0.43	14.18
1.0	16.87	16.87	17.35	9.39	0.56	18.92
1.1	18.87	17.15	19.23	11.23	0.65	23.84
1.2	21.47	17.89	21.67	13.35	0.75	29.37
1.3	26.09	20.07	26.49	15.71	0.78	33.67
1.4	34.16	24.40	34.52	20.21	0.83	42.93
1.5	35.40	23.60	35.88	23.66	1.00	54.45
1.6	36.66	22.91	37.25	27.35	1.19	67.60
1.7	37.85	22.27	38.57	31.14	1.40	81.98
1.8	39.32	21.84	39.99	34.99	1.60	97.21
1.9	39.79	20.94	40.59	38.90	1.86	114.82
2.0	40.44	20.22	41.18	42.95	2.12	134.15
2.1	41.66	19.84	42.45	47.17	2.38	153.68
2.2	42.30	19.23	43.31	51.23	2.66	174.02
2.3	43.00	18.69	44.05	55.50	2.97	196.61
2.4	43.56	18.15	44.35	59.88	3.30	222.15
2.5	44.51	17.80	45.65	64.27	3.61	245.15
2.6	46.37	17.84	47.28	69.02	3.87	269.72
2.7	47.64	17.64	48.72	73.56	4.17	294.02
2.8	48.90	17.47	49.87	78.47	4.49	322.39
2.9	50.01	17.24	51.19	83.44	4.84	350.95
3.0	53.11	17.70	54.27	88.66	5.01	373.43
3.1	54.03	17.43	55.31	93.97	5.39	406.26
3.2	56.73	17.73	58.16	99.32	5.60	430.93

Peak Flood Prediction		
Recurrence Interval (years)	Discharge (m^3s^-1)	Elevation Above Thalweg (m)
2	14.13	0.90
5	34.87	1.31
10	47.12	1.40
25	56.45	1.48
50	59.95	1.53
100	61.78	1.56
200	62.72	1.58
500	63.29	1.60

Site B

Survey Data	
Distance Across Channel (m)	Elevation Above Thalweg (m)
0.00	2.69
0.25	2.59
0.42	2.50
0.57	2.40
0.72	2.28
0.85	2.12
1.17	1.91
1.34	1.76
1.53	1.56
1.65	1.40
1.87	1.30
1.95	1.17
2.04	1.02
2.19	1.01
2.34	0.87
2.49	0.72
2.57	0.61
2.67	0.45
2.80	0.34
2.97	0.29
3.04	0.29
3.17	0.21
3.28	0.15
3.40	0.06
3.47	0.00
3.71	0.07
3.96	0.14
4.21	0.17
4.46	0.15
	4.69
	4.90
	5.12
	5.34
	5.54
	5.74
	5.91
	6.08
	6.31
	6.68
	6.86
	7.03
	7.20
	7.39
	7.56
	7.73
	7.87
	8.05
	8.12
	8.34
	8.60
	8.71
	8.90
	8.95
	9.02
	9.04
	8.93
	8.87
	8.81
	8.71
	0.25
	0.27
	0.33
	0.30
	0.37
	0.34
	0.41
	0.44
	0.46
	0.43
	0.51
	0.63
	0.72
	0.86
	0.85
	0.85
	0.99
	1.01
	1.35
	1.44
	1.30
	1.48
	1.64
	1.90
	2.15
	2.34
	2.55
	2.76
	2.99
	3.18

Schmidt Hammer Q-Value, Elevation Above Thalweg (m)						
0.067 m	0.371 m	0.567 m	0.817 m	1.067 m	2. 067 m	2. 567 m
	34	50.5	42	49	26	22.5
	42	41.5	48	53	40.5	38.5
	20	40.5	51.5	50	39.5	26
	29.5	44	27.5	47.5	43	25.5
	62	47.5	21	49.5	52	43
	21.5	49		40.5		43
	45.5	51.5	60.5	55	60.5	16.5
	56	56	53	66	64	
15.5	28.5	56.5	55.5	54.5	50	30
		62	57.5	57.5	55	20
	23.5	59	62.5	67.5	62.5	23
26.5	44	61	61.5	60	55.5	42.5
22.5	35	63.5	52	67	45	22
15.5		59	64	66	36.5	19
		63	71	57.5	13.5	29
21.5		63	43.5	59	45.5	29.5
16	16	78.5	65	68	34.5	46.5
39	50.5	70	68.5	52.5	22	19
32	41.5	76	69.5	52	43.5	42.5
23	35.5	77	65.5	69	52.5	34.5
18.5		76	48.5	59.5	40.5	41
	45.5	56.5	19.5	52.5	53	42
		27	47.5	46.5	56.5	38.5
	54.5	14.5	63.5	50	40.5	50.5
16	62.5	56.5	61.5	46.5	50.5	17
	61	59	48	51	48.5	16
	51	52	38	58	50	26
	48	57.5	41	54.5	25.5	28
	24.5	52	60	53	43	33
		62		38	44.5	37
	23.5	61	66	21	49	32.5
	39	65	67.5	60		20.5
	45.5	66	70.5	50.5	53	
	57.5	56	66	59.5	32	24
		50.5	68	74.5	53.5	42
	17	44	69	59.5	60.5	50
		53.5	69	71.5	58.5	45
29.5	16	55.5	65	58		52.5
	26.5	53	66.5	55.5	30	53
	21.5	65.5	47.5	62	40.5	54
14		53	55	64.5	59.5	31.5
	50.5	57.5	66	50.5	57.5	41
	37	58	35	66	58	30
	58.5	68.5	38	60	33.5	19
	45	62.5	43	55.5	40	35
	48	55.5	61	50	52	26.5
	55.5	65	54.5	55.5	41.5	
	42.5	73.5	60	62	46.5	30.5
	47.5	69	72.5	57	40.5	ND
	39	61	72	37	43	ND

ND	46.5	48	48	69.5	60	13.5
ND	32.5	69	51	61	44	40
ND	39.5	60.5	61.5	52.5	63.5	54.5
ND		73	55	70.5	47.5	53.5
ND	30.5	44.5	58.5	66	47	53.5
ND	24.5	40	64	57.5	66.5	58.5
ND		71.5	63.5	72	58.5	27
ND		68.5	64.5	73.5	40.5	36.5
ND		47.5	50.5	68.5	53.5	
ND		47	69	58	42	46
ND	32	54	23	68.5	31	38
ND	31	36	33.5	52.5	52.5	51.5
ND		68.5	38	56	47.5	30
ND	16.5	67.5	45	61	23.5	47
ND	41	55.5	62	58.5	49.5	33.5
ND	17	60	55	60	57	51
ND		41.5	70	45	57.5	
ND	14.5	76	54	73	32	44
ND	21	59.5	62.5	65.5	56	14.5
ND	25.5	69.5	64	64	47.5	49
ND	39.5	60.5	45	63	57	
ND		38.5	53	61.5		
ND	51	19	65.5	33	58.5	60
ND		66	63.5	67.5	33.5	64.5
ND	14	64	56.5	56.5	49	43
ND	14	52	71.5	33.5	40.5	56
ND		35	62	61.5	55.5	57
ND	35	61	50.5	39	62	46
ND		58	40	52.5	57	34
ND	37.5	20.5	36	61	74.5	31
ND	33.5	63.5	44.5	51	64.5	34
ND	42.5	70.5	51.5	69.5	42.5	26
ND	50	55.5	58.5	51.5	39.5	33
ND		60	60.5	27.5	68	37
ND	25	62	51	64.5	23	18
ND	58.5	59.5	51	53.5	58	31
ND	63.5	74	54.5	62.5	52.5	56.5
ND		68.5	64	52	25.5	39
ND		58	49	43		55.5
ND		70.5	42	53.5		50.5
ND		68	41	55	62.5	
ND		74.5	32	64.5	52	52
ND	24.5	60.5	63	66	25.5	42.5
ND		59.5	49	68	25.5	46.5
ND	35.5	61.5	70	39	64	51.5
ND	16.5	70.5	65	53	60.5	47
ND		35.5	48.5	60.5	58	59
ND		53.5	70.5	50.5	62.5	32.5
ND		65.5	60.5	56.5	29.5	31
ND		62	68	65.5	18.5	39

Channel Geometry						
Elevation Above Thalweg (m)	Width (m)	Width-to-depth ratio	Wetted Perimeter (m)	Cross Sectional Area (m^2)	Hydraulic Radius (m)	Discharge (m^3s^-1)
0.1	0.47	4.68	0.57	0.02	0.04	0.01
0.2	1.39	6.95	1.49	0.12	0.08	0.11
0.3	2.06	6.87	2.19	0.31	0.14	0.41
0.4	3.15	7.87	3.23	0.60	0.18	0.96
0.5	4.20	8.39	4.32	0.98	0.23	1.81
0.6	4.40	7.34	4.65	1.40	0.30	3.11
0.7	4.65	6.65	4.99	1.87	0.37	4.80
0.8	4.89	6.12	5.38	2.35	0.44	6.68
0.9	5.47	6.08	6.11	2.88	0.47	8.62
1.0	5.76	5.76	6.43	3.45	0.54	11.24
1.1	6.08	5.52	7.00	4.04	0.58	13.86
1.2	6.16	5.13	7.04	4.64	0.66	17.38
1.3	6.24	4.80	7.06	5.27	0.75	21.49
1.4	6.60	4.71	7.70	6.06	0.79	25.57
1.5	7.17	4.78	8.67	6.70	0.77	27.91
1.6	7.37	4.61	8.66	7.47	0.86	33.48
1.7	7.52	4.42	9.18	8.10	0.88	36.90
1.8	7.64	4.24	9.22	8.95	0.97	43.45
1.9	7.77	4.09	9.80	9.68	0.99	47.48
2.0	7.95	3.97	9.87	10.50	1.06	54.14
2.1	8.13	3.87	9.95	11.30	1.14	60.89
2.2	8.24	3.75	10.44	12.26	1.17	67.53
2.3	8.35	3.63	10.48	12.94	1.24	73.75
2.4	8.45	3.52	10.96	13.84	1.26	80.03
2.5	8.53	3.41	11.02	14.75	1.34	88.65
2.6	8.70	3.35	11.61	15.62	1.35	94.18

Peak Flood Prediction				
Recurrence Interval (years)	Discharge (m^3s^-1)	Standard Error of Prediction (%)	Standard Error of Prediction (+/- m^3s^-1)	Peak Flood Elevation Above Thalweg (m)
2	9.77	33.4	3.26	0.95
5	19.44	34.1	6.63	1.25
10	28.05	35.5	9.96	1.49
25	41.30	38.8	16.03	1.75
50	52.88	42.2	22.32	1.95
100	65.77	46.2	30.39	2.20
200	80.34	50.7	40.73	2.40
500	101.98	56.7	57.83	2.65

Site C

Survey Data			
Distance Across Channel (m)	Elevation Above Thalweg (m)		
0.00	1.62	4.00	0.20
0.22	1.54	4.28	0.17
0.44	1.43	4.56	0.12
0.66	1.33	4.78	0.10
0.72	1.15	4.95	0.04
0.75	0.91	5.13	0.03
0.89	0.68	5.34	0.00
1.08	0.66	5.57	0.00
1.25	0.54	5.73	0.16
1.47	0.43	5.85	0.37
1.71	0.38	5.75	0.53
1.95	0.32	5.78	0.74
2.21	0.20	6.03	0.80
2.45	0.20	6.22	0.76
2.71	0.17	6.40	0.91
3.00	0.16	6.61	1.04
3.23	0.24	6.82	1.12
3.47	0.23	7.02	1.30
3.74	0.20	7.25	1.49
		7.53	1.80
		7.72	1.99

Schmidt Hammer Q-Value, Elevation Above Thalweg (m)					
0.1 m	0.4 m	0.6 m	0.9m	1.1 m	1.6 m
68.5	31				
30	33				
	46.5	18			
44.5					
	31.5				
	25.5	16.5			
	61.5	32.5			
45	45.5				
46	19	13.5			
37					
51	28				
48	15.5				
54.5	33	38			
		15			
		39.5			
24.5					
34	22				
	55				
17.5	55.5				
16.5					
35	23				
17					
	30				
	28.5				
17					
	36				
	41				
	39.5				
	46	38.5			
	39.5				
		33	24.5		

	58.5	39	34.5	53	50
	60	44	30.5	44.5	43.5
	58	37.5	43.5	40	28
56	58.5	60	39	25.5	48
	59	42	55.5	39.5	59.5
	49	43	41	39	32.5
57.5	34	44	46	46.5	70
18		45	48.5	54	42
	45	48		52.5	56
69.5	45.5	38	45.5	48	27.5
66	65	51.5	38.5	48	40.5
59.5	23.5	43.5	59.5	41.5	29.5
53	63	45.5	54	39	33.5
34	58	56	52.5	22	31
37.5	63	57	56.5	29.5	23.5
56.5	63.5	57	31	31	39
64	60	44.5		37.5	27
	54.5	67.5		36.5	28.5
33	54	32		24	30
	26	50	65.5	36.5	28
60		46	70.5	53.5	41.5
52.5	44	45	43	51	39.5
55	17	36	53.5	46.5	32
57.5	58.5	16	34.5	37.5	33
57	64.5	51	53	56.5	34
55	44.5		48.5	52	27.5
68.5	66.5	52.5	26	28	34.5
48.5	54.5	66.5	51.5	57	35.5
39.5	72.5	60.5	46	27.5	22.5
	64	40.5	46	19	34.5
65.5	65.5	61	39	40	27.5
61	63.5	48.5	41.5	53.5	33
	67.5	59.5	16	55.5	35.5
52	60.5	68	36	57	32
41	57	49	33		27
	45.5	63.5	40.5	54.5	
32	63	52	64.5	53.5	29.5
	43	63		53	41.5
	37.5	54.5	67.5	35.5	47
20.5	40.5	51.5	54	41	57
62.5	49	29	53.5	45	52
46	64	47.5	29	58	58
	55.5	44	51	39.5	48
41.5	66.5	48	61	54	41.5
	55.5	44.5	53	56.5	40.5
62	51.5	45	59.5	38.5	23
	64	39.5	55.5	44.5	
	67.5	33	59.5	31	41
	52.5	45.5	57	21.5	43
	54	66	59.5	30	51.5

Channel Geometry						
Elevation Above Thalweg (m)	Width (m)	Width-to-depth ratio	Wetted Perimeter (m)	Cross Sectional Area (m^2)	Hydraulic Radius (m)	Discharge (m^3s^-1)
0.1	0.23	2.28	0.29	0.01	0.05	0.00
0.2	1.62	8.08	1.94	0.15	0.08	0.03
0.3	3.68	12.26	3.90	0.47	0.12	0.12
0.4	4.07	10.18	4.58	0.89	0.19	0.31
0.5	4.39	8.78	4.78	1.31	0.28	0.58
0.6	4.59	7.65	5.26	1.77	0.34	0.90
0.7	4.90	7.00	5.46	2.27	0.42	1.33
0.8	5.02	6.27	5.73	2.76	0.48	1.78
0.9	5.17	5.75	5.99	3.25	0.54	2.27
1.0	5.23	5.23	6.33	3.78	0.60	2.82
1.1	5.29	4.81	6.55	4.30	0.66	3.42
1.2	5.35	4.46	6.83	4.81	0.70	4.00
1.3	5.42	4.17	6.84	5.36	0.78	4.79
1.4	5.61	4.00	7.29	5.92	0.81	5.42
1.5	5.84	3.89	7.96	6.58	0.83	6.09
1.6	6.10	3.81	8.12	7.20	0.89	6.98

Peak Flood Prediction				
Recurrence Interval (years)	Discharge (m^3s^-1)	Standard Error of Prediction (%)	Standard Error of Prediction (+/- m^3s^-1)	Peak Flood Elevation Above Thalweg (m)
2	2.88	45.0	1.30	1.00
5	5.37	43.4	2.33	1.40
10	7.45	44.2	3.29	1.60
25	10.37	46.6	4.83	1.95
50	12.88	49.1	6.33	2.20
100	15.68	52.0	8.15	2.40
200	18.71	55.3	10.35	2.60
500	23.14	60.2	13.93	2.95

Site D

Survey Data		
Distance Across Channel (m)	Elevation Above Thalweg (m)	Schmidt Hammer Q-Value
0	1.20	61.3
0.1	1.16	52.5
0.2	0.96	55.2
0.3	0.90	63.1
0.4	0.83	55.2
0.5	0.73	55.6
0.6	0.61	50.6
0.7	0.52	60.5
0.8	0.43	55.2
0.9	0.34	ND
1	0.23	ND
1.1	0.06	ND
1.2	0.00	ND
1.3	0.12	ND
1.4	0.25	37.6
1.5	0.37	53.9
1.6	0.45	54.3
1.7	0.55	58.6
1.8	0.64	56.1
1.9	0.85	62.0
2	0.96	56.5
2.1	1.06	60.9
2.2	1.17	53.9
2.3	1.25	60.1

Channel Geometry						
Elevation Above Thalweg (m)	Width (m)	Width-to-depth ratio	Wetted Perimeter (m)	Cross Sectional Area (m^2)	Hydraulic Radius (m)	Discharge (m^3s^-1)
0.1	0.20	1.99	0.15	0.02	0.14	0.06
0.2	0.35	1.75	0.43	0.07	0.16	0.22
0.3	0.46	1.55	0.68	0.14	0.21	0.51
0.4	0.52	1.30	0.90	0.21	0.23	0.83
0.5	0.59	1.19	1.11	0.30	0.27	1.30
0.6	0.66	1.10	1.31	0.40	0.30	1.89
0.7	0.63	0.90	1.61	0.44	0.27	1.97
0.8	0.65	0.81	1.63	0.52	0.32	2.56
0.9	0.64	0.71	1.97	0.58	0.29	2.67
1.0	0.75	0.75	2.27	0.75	0.33	3.75
1.1	0.77	0.70	2.48	0.84	0.34	4.34
1.2	0.80	0.67	2.71	0.96	0.36	5.11

Site E

Survey Data		
Distance Across Channel (m)	Elevation Above Thalweg (m)	Schmidt Hammer Q-Value
0.00	2.61	26.5
0.16	2.53	
0.15	2.48	23.5
0.22	2.37	20
0.23	2.30	
0.29	2.20	34.5
0.32	2.13	19
0.36	2.05	37.5
0.35	1.96	33
0.40	1.88	
0.45	1.81	34.5
0.47	1.72	33
0.53	1.63	33
0.60	1.60	33.5
0.68	1.54	
0.74	1.48	28.5
0.79	1.40	45.5
0.86	1.36	36
0.93	1.30	33
0.98	1.23	27
1.02	1.17	33
1.09	1.13	26.5
1.15	1.06	45.5
1.19	0.99	26.5
1.22	0.91	
1.30	0.88	
1.40	0.83	42.5
1.43	0.76	31.5
1.45	0.70	41
1.55	0.67	
1.59	0.59	18.5
1.68	0.53	
1.73	0.49	48.5
1.84	0.41	51.5
1.91	0.41	41.5
2.02	0.37	42
2.09	0.34	45
2.19	0.30	19.5
2.27	0.27	42.5
2.36	0.21	44.5
2.42	0.20	48.5
2.56	0.18	36.5
2.67	0.17	32.5
2.78	0.19	23.5
2.85	0.14	41
2.98	0.18	32
3.02	0.17	49
3.12	0.15	ND
3.21	0.13	ND

3.30	0.13	ND
3.41	0.09	ND
3.47	0.05	ND
3.57	0.05	ND
3.63	0.04	ND
3.78	0.06	ND
3.87	0.06	ND
4.03	0.06	33.5
4.07	0.05	31.5
4.15	0.05	39.5
4.26	0.05	49
4.34	0.05	30
4.36	0.04	50
4.39	0.04	42.5
4.45	0.03	
4.50	0.03	
4.56	0.05	ND
4.59	0.04	ND
4.67	0.04	ND
4.72	0.03	28.5
4.90	0.03	ND
5.04	0.03	ND
5.12	0.02	ND
5.24	0.02	ND
5.32	0.02	ND
5.43	0.00	ND
5.52	0.00	ND
5.63	0.00	ND
5.73	0.00	ND
5.86	0.00	ND
5.98	0.02	50.5
6.05	0.02	45
6.04	0.04	44.5
6.14	0.03	56
6.23	0.03	50
6.31	0.03	54
6.46	0.03	41
6.50	0.04	41
6.60	0.04	43
6.67	0.04	37.5
6.75	0.03	42.5
6.82	0.03	47
6.90	0.05	34.5
7.00	0.05	23
7.10	0.05	45
7.22	0.04	55.5
7.26	0.04	48
7.39	0.06	43
7.44	0.05	50.5
7.55	0.07	52.5
7.65	0.06	51.5
7.75	0.06	38
7.80	0.06	49.5

7.92	0.05	48
8.04	0.03	40.5
8.10	0.04	42.5
8.19	0.04	24.5
8.26	0.04	44.5
8.38	0.02	
8.49	0.05	19.5
8.56	0.06	
8.66	0.07	
8.78	0.07	
8.86	0.08	28.5
8.95	0.10	19
9.06	0.10	29
9.17	0.13	24
9.25	0.15	37.5
9.35	0.17	39
9.43	0.21	26.5
9.55	0.27	21
9.65	0.34	27
9.72	0.37	27.5
9.79	0.41	48
9.89	0.47	25
9.95	0.50	26.5
10.04	0.57	27.5
10.13	0.61	28.5
10.24	0.63	32
10.29	0.63	18
10.39	0.67	17.5
10.40	0.76	26.5
10.48	0.80	26
10.56	0.83	28.5
10.67	0.85	28
10.78	0.90	31.5
10.85	0.97	28
10.92	1.01	37
11.00	1.05	30
11.08	1.12	36.5
11.17	1.16	31.5
11.18	1.20	ND
11.18	1.33	
11.18	1.38	
11.22	1.47	42
11.27	1.58	23.5
11.33	1.65	21.5
11.38	1.66	
11.52	1.73	26
11.57	1.77	20.5
11.66	1.77	26.5

Channel Geometry						
Elevation Above Thalweg (m)	Width (m)	Width-to-depth ratio	Wetted Perimeter (m)	Cross Sectional Area (m^2)	Hydraulic Radius (m)	Discharge (m^3s^-1)
0.1	4.68	46.81	4.73	0.29	0.06	0.25
0.2	5.98	29.88	6.12	0.83	0.14	1.19
0.3	6.35	21.15	6.60	1.46	0.22	2.89
0.4	6.73	16.83	6.99	2.11	0.30	5.16
0.5	7.10	14.19	7.39	2.83	0.38	8.10
0.6	7.32	12.20	7.71	3.56	0.46	11.52
0.7	7.70	11.00	8.24	4.31	0.52	15.21
0.8	7.81	9.76	8.38	5.08	0.61	19.75
0.9	8.23	9.15	8.86	5.92	0.67	24.57
1.0	8.39	8.39	9.18	6.72	0.73	29.60
1.1	8.60	7.82	9.48	7.58	0.80	35.42
1.2	8.76	7.30	10.02	8.47	0.85	41.10
1.3	8.87	6.82	10.04	9.37	0.93	48.57
1.4	8.99	6.42	10.49	10.30	0.98	55.23
1.5	9.11	6.08	10.72	11.22	1.05	62.80
1.6	9.26	5.79	11.00	12.23	1.11	71.22
1.7	9.52	5.60	11.29	13.23	1.17	79.82

Peak Flood Prediction				
Recurrence Interval (years)	Discharge (m^3s^-1)	Standard Error of Prediction (%)	Standard Error of Prediction (+/- m^3s^-1)	Peak Flood Elevation Above Thalweg (m)
2	13.92	108	15.04	0.65
5	32.47	80	25.98	1.05
10	49.75	70	34.82	1.30
25	80.22	62	49.74	1.70
50	108.80	60	65.28	1.95
100	150.11	61	91.57	2.30
200	179.95	62	111.57	2.55
500	241.24	66	159.22	3.00

Site F

Survey Data		
Distance Across Channel (m)	Elevation Above Thalweg (m)	Schmidt Hammer Q-Value
0	3.23	20
0.1	3.12	20
0.2	3.04	24.5
0.3	2.94	23
0.4	2.85	23
0.5	2.73	21.5
0.6	2.65	
0.7	2.61	27.5
0.8	2.49	16.5
0.9	2.47	21
1	2.39	20.5
1.1	2.34	19
1.2	2.33	18
1.3	2.27	21
1.4	2.23	29
1.5	2.17	19.5
1.6	2.07	29.5
1.7	1.97	
1.8	1.88	
1.9	1.80	
2	1.68	
2.1	1.62	22.5
2.2	1.55	
2.3	1.50	44.5
2.4	1.48	40.5
2.5	1.42	34
2.6	1.40	31.5
2.7	1.35	40.5
2.8	1.26	51.5
2.9	1.16	45
3	1.05	21
3.1	1.04	24
3.2	1.12	38.5
3.3	1.12	27.5
3.4	1.18	27.5
3.5	1.18	42.5
3.6	1.18	34.5
3.7	1.10	41
3.8	1.04	44.5
3.9	0.94	59
4	0.94	52
4.1	0.93	57.5
4.2	0.96	53
4.3	0.94	38.5
4.4	0.95	49.5
4.5	0.95	57
4.6	0.95	32
4.7	0.95	41.5
4.8	0.93	46
4.9	0.92	39.5
5	0.89	46
5.1	0.92	46

5.2	0.90	57.5
5.3	0.91	55.5
5.4	0.89	43.5
5.5	0.90	61
5.6	0.90	51
5.7	0.82	41.5
5.8	0.78	41.5
5.9	0.76	52
6	0.76	52.5
6.1	0.73	35.5
6.2	0.65	46.5
6.3	0.61	53.5
6.4	0.58	55.5
6.5	0.57	57
6.6	0.54	66.5
6.7	0.50	50.5
6.8	0.47	60.5
6.9	0.42	42.5
7	0.37	40.5
7.1	0.33	57
7.2	0.33	50.5
7.3	0.29	44
7.4	0.28	43.5
7.5	0.20	
7.6	0.10	47
7.7	0.00	ND
7.8	0.01	
7.9	0.02	48
8	0.03	57
8.1	0.05	42.5
8.2	0.07	52.5
8.3	0.08	55.5
8.4	0.10	49
8.5	0.10	48.5
8.6	0.05	62.5
8.7	0.06	45
8.8	0.08	54
8.9	0.10	51
9	0.13	64
9.1	0.15	60
9.2	0.15	38.5
9.3	0.13	44.5
9.4	0.15	55
9.5	0.15	55
9.6	0.16	46.5
9.7	0.18	50.5
9.8	0.13	45.5
9.9	0.16	56.5
10	0.17	43
10.1	0.13	43.5
10.2	0.13	35.5
10.3	0.11	ND
10.4	0.12	ND
10.5	0.13	ND
10.6	0.12	ND
10.7	0.06	ND
10.8	0.06	ND

10.9	0.04	ND
11	0.08	ND
11.1	0.03	ND
11.2	0.07	ND
11.3	0.07	ND
11.4	0.11	48
11.5	0.14	53
11.6	0.14	47.5
11.7	0.13	56
11.8	0.30	56
11.9	0.29	
12	0.35	58.5
12.1	0.38	45.5
12.2	0.42	42.5
12.3	0.47	43.5
12.4	0.48	45.5
12.5	0.55	57
12.6	0.58	56
12.7	0.68	40.5
12.8	0.73	54
12.9	0.79	66
13	0.79	63
13.1	0.84	36.5
13.2	0.89	49
13.3	1.02	48
13.4	1.11	61
13.5	1.18	15.5
13.6	1.24	
13.7	1.28	43.5
13.8	1.46	54
13.9	1.54	
14	1.57	16
14.1	1.64	40
14.2	1.62	39
14.3	1.66	53.5
14.4	1.95	55
14.5	2.05	45.5
14.6	2.07	37.5
14.7	2.19	22
14.8	2.27	35.5
14.9	2.37	
15	2.44	25
15.1	2.44	25

Channel Geometry						
Elevation Above Thalweg (m)	Width (m)	Width-to-depth ratio	Wetted Perimeter (m)	Cross Sectional Area (m^2)	Hydraulic Radius (m)	Discharge (m^3s^-1)
0.1	1.19	11.85	1.37	0.05	0.04	0.02
0.2	4.40	22.00	4.77	0.44	0.09	0.35
0.3	4.59	15.31	4.81	0.90	0.19	1.16
0.4	5.05	12.64	5.68	1.41	0.25	2.17
0.5	5.44	10.87	6.24	1.95	0.31	3.52
0.6	5.92	9.86	6.78	2.53	0.37	5.15
0.7	6.08	8.68	7.00	3.15	0.45	7.25
0.8	6.58	8.23	7.65	3.82	0.50	9.41
0.9	6.78	7.53	8.05	4.48	0.56	11.88
1.0	8.50	8.50	9.65	5.37	0.56	14.24
1.1	8.56	7.78	9.92	6.20	0.62	17.73
1.2	8.98	7.49	10.98	7.15	0.65	21.01
1.3	9.17	7.05	11.38	8.13	0.71	25.42
1.4	8.98	6.42	11.59	9.23	0.80	31.08
1.5	8.72	5.81	12.07	10.18	0.84	35.58
1.6	8.72	5.45	12.45	11.25	0.90	41.18
1.7	8.89	5.23	13.11	12.28	0.94	46.03
1.8	8.86	4.92	13.10	13.39	1.02	53.16
1.9	8.78	4.62	13.13	14.54	1.11	60.90
2.0	8.83	4.41	13.55	15.62	1.15	67.24
2.1	8.84	4.21	13.83	16.72	1.21	74.27
2.2	8.91	4.05	14.04	17.85	1.27	82.01
2.3	9.04	3.93	14.35	19.06	1.33	90.15
2.4	9.36	3.90	14.71	20.29	1.38	98.44

Peak Flood Prediction				
Recurrence Interval (years)	Discharge (m^3s^-1)	Standard Error of Prediction (%)	Standard Error of Prediction (+/- m^3s^-1)	Peak Flood Elevation Above Thalweg (m)
2	8.09	108	8.73	0.8
5	20.96	80	16.76	1.2
10	33.87	70	23.71	1.5
25	57.53	62	35.67	1.9
50	80.55	60	48.33	2.2
100	111.60	61	68.07	2.5
200	140.12	62	86.88	2.8
500	193.31	66	127.58	3.4